

# Comparison of temperature dependent calibration methods of an instrument to measure OH and HO<sub>2</sub> radicals using laser-induced fluorescence spectroscopy

Frank A. F. Winiberg<sup>1,2</sup>, William J. Warman<sup>1</sup>, Charlotte A. Brumby<sup>1</sup>, Graham Boustead<sup>1</sup>, Iustinian G. Bejan<sup>1,3</sup>, Thomas H. Speak<sup>1</sup>, Dwayne E. Heard<sup>1</sup>, Daniel Stone<sup>1</sup> and Paul W. Seakins<sup>1</sup>

[1] School of Chemistry, University of Leeds, Leeds, LS2 9JT, United Kingdom

[2] Now at: NASA's Jet Propulsion Laboratory, California Institute of Technology, Pasadena, 91109, USA

[3] Now at: Faculty of Chemistry and "Integrated Centre for Environmental Science Studies in the North-East Development Region – CERNESIM", "Al. I. Cuza" University of Iasi, Romania

*Correspondence to:* Paul W. Seakins ([p.w.seakins@leeds.ac.uk](mailto:p.w.seakins@leeds.ac.uk))

## Abstract

Laser Induced Fluorescence (LIF) spectroscopy has been widely applied to fieldwork measurements of OH radicals, and of HO<sub>2</sub>, following conversion to OH, over a wide variety of conditions, on different platforms, and in simulation chambers. Conventional calibration of HO<sub>x</sub> (OH + HO<sub>2</sub>) instruments has mainly relied on a single method, generating known concentrations of HO<sub>x</sub> from H<sub>2</sub>O vapour photolysis in a flow of zero air impinging just outside the sample inlet ( $S_{HO_x} = C_{HO_x} \cdot [HO_x]$ , where  $S_{HO_x}$  is the observed signal and  $C_{HO_x}$  is the calibration factor). The FAGE (Fluorescence Assay by Gaseous Expansion) apparatus designed for HO<sub>x</sub> measurements in the Highly Instrumented Reactor for Atmospheric Chemistry (HIRAC) at the University of Leeds has been used to examine the sensitivity of FAGE to external gas temperatures (266 – 348 K).

The conventional calibration methods give the temperature dependence of  $C_{OH}$  (relative to the value at 293 K) of  $(0.0059 \pm 0.0015) \text{ K}^{-1}$  and  $C_{HO_2}$  of  $(0.014 \pm 0.013) \text{ K}^{-1}$ . Errors are  $2\sigma$ .  $C_{OH}$  was also determined by observing the decay of hydrocarbons (typically cyclohexane) caused by OH reactions giving  $C_{OH}$  (again, relative to the value at 293 K) of  $(0.0038 \pm 0.0007) \text{ K}^{-1}$ . Additionally,  $C_{HO_2}$  was determined based on the second order kinetics of HO<sub>2</sub> recombination with the temperature dependence of  $C_{HO_2}$ , relative to 293 K being  $(0.0064 \pm 0.0034) \text{ K}^{-1}$ .

1 The temperature dependence of  $C_{\text{HOx}}$  depends on HOx number density, quenching, relative  
2 population of the probed OH rotational level and HOx transmission from inlet to detection axis.  
3 The first three terms can be calculated and, in combination with the measured values of  $C_{\text{HOx}}$ ,  
4 show that HOx transmission increases with temperature. Comparisons with other instruments  
5 and the implications of this work are discussed.

6

## 7 **1 Introduction**

8 Hydroxyl radicals (OH) play a key role in our atmosphere, oxidising a broad range of species.  
9 OH is the main daytime oxidant in the troposphere and the main sink for methane, a potent  
10 greenhouse gas. The OH radical is linked to the HO<sub>2</sub> radical through the oxidation of most  
11 other non-methane hydrocarbons (NMHCs) and CO in the troposphere and, through reaction  
12 with NO<sub>2</sub>, in the upper troposphere/lower stratosphere. Due to the high reactivity of OH  
13 (lifetime ~1 s even in clean air), these radicals undergo minimal transport and local  
14 concentrations depend only on the *in situ* chemistry. Measurements of HOx concentrations, in  
15 conjunction with measurements of their sources and sinks are a sensitive test of chemical  
16 models. Accurate measurement of [HOx] is therefore paramount, not only for field  
17 measurements, (Stone et al., 2012; Heard and Pilling, 2003; Gligorovski et al., 2015), but also  
18 for atmospheric simulation chambers where OH/HO<sub>2</sub> instruments have been deployed (Karl et  
19 al., 2004; Glowacki et al., 2007).

20 Sensitive detection techniques with high temporal resolution are required for HOx detection  
21 and techniques have been reviewed in Stone et al. (2012) and Wang et al. (2021). Fluorescence  
22 Assay by Gaseous Expansion (FAGE) (e.g. Hard et al. (1984)) is the most common method  
23 used for both field and chamber studies. Here, the sample is expanded to low pressures and OH  
24 detected by resonance fluorescence at ~308 nm. The low pressures are required to temporally  
25 separate fluorescence from the excitation laser pulse. HO<sub>2</sub> is converted to OH by reaction with  
26 NO and detected in a separate cell. Both techniques require calibration which is conventionally  
27 based on the generation of OH and HO<sub>2</sub> from water vapour photolysis at 185 nm at atmospheric  
28 temperature and pressure.

29 Recent studies have demonstrated potential interferences for measurements of both OH and  
30 HO<sub>2</sub> radicals using the FAGE technique, with the magnitude dependent upon instrument design  
31 (Mao et al., 2012; Novelli et al., 2014; Novelli et al., 2017; Fuchs et al., 2011; Whalley et al.,  
32 2013; Fuchs et al., 2016; Fittschen et al., 2019). Considerable effort has been made to minimize,

1 understand and mitigate any interference, with many groups now fitting an external OH  
2 scavenger injector to measure OH concentrations using an alternative background signal,  
3 OH<sub>CHEM</sub>, alongside the conventional method of measuring OH using a background signal  
4 determined by tuning the laser wavelength off-resonant to the transition, OH<sub>WAVE</sub> (Woodward-  
5 Massey et al., 2020;Novelli et al., 2014;Mao et al., 2012). Intercomparison campaigns (e.g.  
6 Schlosser et al. (2009), Onel et al. (2017a)) in the controlled environment of an atmospheric  
7 chamber are useful to identify systematic errors in different approaches, but if both methods  
8 require calibration, the accuracy of the measurements is still compromised by uncertainties in  
9 the calibration methods.

10 In an earlier paper (Winiberg et al., 2015), accurate calibration of a FAGE instrument over  
11 a range of external inlet pressures (440 – 1000 mbar) was performed in the Leeds HIRAC  
12 (Highly Instrumented Reactor for Atmospheric Chemistry (Glowacki et al., 2007)) chamber.  
13 The instrument sensitivity to OH and HO<sub>2</sub> agreed well for the conventional water vapour  
14 calibration method (where the external pressure is always 1 bar, and external pressure effects  
15 were simulated by altering the pressure in the FAGE detection cell) and alternative methods  
16 based on the temporal decay of a hydrocarbon (for OH) or the temporal decay of HO<sub>2</sub> via its  
17 second-order self-reaction (for HO<sub>2</sub>) over an external pressure range of 300 – 1000 mbar. For  
18 OH, the calibration factor,  $C_{OH}$ , (where  $S_{HOx} = C_{HOx} \cdot [HOx]$  and  $S_{HOx}$  is the FAGE signal)  
19 increased by 17% and for HO<sub>2</sub> a slightly greater increase in  $C_{HO2}$  of 32% was determined as  
20 the pressure increased from 350 to 1000 mbar. There was good agreement between the absolute  
21 values and their pressure dependence for both calibration methods. Such comparisons are  
22 particularly relevant to aircraft operation where external pressures will vary considerably  
23 during the flight or for evacuable chambers such as the Leeds HIRAC chamber which can  
24 operate from 50 – 1000 mbar. Marno et al. (2020) have also developed the All Pressure  
25 Altitude-based Calibrator of HO<sub>x</sub> Experimentation (APACHE) to allow calibration of their  
26 FAGE instrument HORUS (HydrOxyl Radical measurement Unit based on fluorescence  
27 Spectroscopy) as a function of pressure, but not temperature.

28 Little is known on the effect of gas temperature at the inlet upon instrument sensitivity for  
29 LIF instruments, despite field instruments being used at extremes of temperature, from day to  
30 night, from deserts to the polar regions, and in aircraft, where temperatures change rapidly with  
31 altitude. Additionally, ambient conditions influence not only the inlet temperature, but the  
32 whole apparatus. For example in the FAGE system associated with HIRAC, based on a design  
33 for aircraft use (Commane et al., 2010), the whole inlet tube (~30 cm) is located inside the

1 HIRAC chamber and so wall loss rates of HO<sub>x</sub> in the inlet tube will be influenced by the  
 2 temperature of the HIRAC chamber. The long inlet is required either to locate the pinhole  
 3 outside of the aircraft for the airborne instrument, or to allow sampling across the diameter of  
 4 the HIRAC chamber. To date, the only study investigating the effect of inlet temperature on  
 5 instrument sensitivity to HO<sub>x</sub> radicals has been performed by Regelin et al. (2013), who  
 6 reported a minor positive dependence of the OH sensitivity ( $C_{OH}$ ) as a function of decreasing  
 7 inlet temperature for the HORUS instrument (possibly due to a cooling effect on the  
 8 instrumentation). There was a more marked decrease in the instrument sensitivity to HO<sub>2</sub> with  
 9 decreasing temperature, most probably due to enhanced wall losses at lower temperatures.

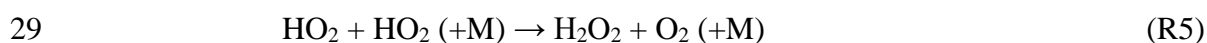
10 In this paper, instrument sensitivity as a function of external inlet temperature has been  
 11 determined for the HIRAC FAGE instrument for both OH and HO<sub>2</sub>, using the water vapour  
 12 photolysis calibration method in an external flowtube (termed ‘conventional method’) and  
 13 alternative calibration methods using chemical reactions in the HIRAC chamber (Winiberg et  
 14 al., 2015) at varying temperatures. Alternative OH calibrations used the inferred [OH] from the  
 15 measured decay of a hydrocarbon (HC), typically cyclohexane, reacting with OH (R1) (termed  
 16 ‘HC decay method’). The rate of loss of HC is then given by equation (E1).



$$18 \quad \frac{-d[\text{HC}]}{dt} = k_{bi}[\text{OH}][\text{HC}] \quad (\text{E1})$$

19 In E(1),  $k_{bi}$  is the well-established literature value for the bimolecular rate coefficient between  
 20 OH and the monitored hydrocarbon and  $\frac{-d[\text{HC}]}{dt}$  can be measured from the HC time series so  
 21 that [OH] is the only unknown parameter and can be calculated and compared with the [OH]  
 22 predicted via the conventional calibration method.

23 HO<sub>2</sub> was also calibrated by monitoring the HO<sub>2</sub> kinetic decay during the recombination  
 24 following generation by HCHO photolysis in the presence of O<sub>2</sub> (termed ‘HO<sub>2</sub> self-reaction  
 25 method’).



1 The time dependence of the  $[\text{HO}_2]$  in the second-order decay depends on the initial  
2 concentration of  $\text{HO}_2$  allowing for calibration.

3

## 4 **2 Experimental**

### 5 **2.1 The HIRAC chamber**

6 The alternative calibration methods of monitoring hydrocarbon or  $\text{HO}_2$  decays were conducted  
7 in HIRAC using very similar methods and conditions as described in Winiberg et al. (2015).  
8 HIRAC is a stainless steel chamber with a total volume of  $2.25 \text{ m}^3$  and can operate over a wide  
9 range of pressures (50 – 1000 mbar) and temperatures (227 – 343 K). Multiple access ports are  
10 available to connect an array of instrumentation and monitoring equipment (pressure gauges,  
11 thermocouples etc.). The chamber has been described previously in detail in Glowacki et al.  
12 (2007), Malkin et al. (2010) and (Bejan et al., 2018). More recently a temperature control  
13 system was installed to further enhance the capabilities of the HIRAC chamber (Section 2.1.1).  
14 Details on the temperature characteristics of HIRAC can be found in Section S1 of the SI.

15 The photolysis lamps, housed in eight quartz tubes mounted radially inside the reactive  
16 volume, were used to initiate photochemistry. The lamps were interchangeable depending on  
17 the target molecules; lamps, with primary emissions centred at 254 and 310 nm (GE Optica,  
18 GE55T8/HO and Philips, TL40W/12 RS respectively), were used for the alternative OH and  
19  $\text{HO}_2$  calibration methods respectively (sections 3.2 and 3.3). The housings were flushed with  
20 dry  $\text{N}_2$  (~3 slm per housing) to help regulate the temperature and remove photolabile species  
21 and water, which could condense or freeze around the lamps at lower temperatures. A  
22 photolysis lamp induced chamber temperature increase of ~2 – 5 K was seen over the course  
23 of a typical experiment (<40 mins), but this variation was reduced if the chamber was  
24 temperature controlled. Temperatures were monitored using a series of K-type thermocouples  
25 inside the lamp housings (one per lamp) as well as distributed around the inside of the chamber.  
26 Thermocouples were placed strategically to allow the temperature to be measured close to the  
27 chamber walls, inlets, flanges and in the chamber.

#### 28 **2.1.1 Temperature Control System**

29 During manufacture, square cross section steel tubing (volume ~50 L) was welded directly to  
30 the outer skin of HIRAC, allowing a cooling/heating liquid to flow around the chamber,

1 controlling the temperature inside. The square tubing enabled the temperature control liquid to  
2 transfer heat more efficiently to the chamber by offering a larger contact surface area compared  
3 to cylindrical tubing. A Huber thermostat unit (model 690W) was used to circulate ~60 L of  
4 thermofluid (Huber DW-THERM, 183 - 473 K) around the chamber. Further details are given  
5 in the SI (Section S1).

6 HIRAC was able to sustain a steady temperature ( $\pm 2$  K) across the chamber at any  
7 temperature between 227 and 343 K and example temperature profiles are given in the SI . A  
8 negligible temperature gradient ( $< 0.5$  K, see Figure S2) was observed across the central portion  
9 of the chamber, in both the horizontal and vertical axes. Close to the walls of the chamber,  
10 however, a change of  $\sim 1$  K was observed. The flanges around the HIRAC chamber were  
11 insulated with  $\sim 40$  mm of neoprene, however there was no direct temperature control of the  
12 flanges or access ports, which was likely responsible for the change in temperature at the large  
13 600 mm access flanges.

#### 14 2.1.2 HO<sub>x</sub> Instrumentation

15 The OH and HO<sub>2</sub> radicals were detected using a FAGE instrument based in the HIRAC  
16 chamber with a 5 kHz pulse repetition frequency (PRF) laser light source, as described in  
17 Winiberg et al. (2015); Winiberg et al. (2016) and Glowacki et al. (2007). Air was sampled at  
18  $\sim 6$  slm through a 1.0 mm diameter pinhole nozzle and passed down the inlet (length 280 mm,  
19 50 mm diameter) into the OH detection axis maintained at low pressure (typically  $\sim 3.85$  mbar)  
20 using a high-capacity rotary-backed roots blower pumping system (Leybold, Trivac D40B and  
21 Ruvac WAU251). The long inlet was used to draw a sample away from the chamber walls  
22 where radical losses increase (a maximum of 15% decrease at  $< 10$  mm from the chamber wall)  
23 and to probe any radical gradients occurring due to spatially inhomogeneous production  
24 (Winiberg et al., 2015). The FAGE instrument was coupled to the HIRAC chamber using ISO-  
25 K160 flanges, ensuring the pinhole is kept  $> 200$  mm from the chamber walls.

26 Concentrations of HO<sub>2</sub> were measured simultaneously in a second detection axis  $\sim 300$  mm  
27 downstream of the OH detection axis. High purity NO (BOC, N2.5 Nitric Oxide) was added  
28  $\sim 20$  mm before the HO<sub>2</sub> detection axis into the centre of the FAGE cell in the direction of gas  
29 flow through 1/8" stainless steel tubing at a rate of 5 sccm (Brooks 5850S) converting HO<sub>2</sub> to  
30 OH. Conversion of some types of RO<sub>2</sub> radicals (in particular  $\beta$ -hydroxyperoxy radicals) to OH  
31 upon reaction with NO has been reported in other FAGE instruments (Whalley et al.,  
32 2013; Fuchs et al., 2011). However, during the alternative HO<sub>2</sub> calibrations (based on HCHO

1 photolysis) presented here no  $\beta$ -hydroxyperoxy radicals were generated hence any interference  
2 was assumed to be negligible.

3 A JDSU Nd:YAG pumped Sirah Cobra Stretch system (PRF = 5 kHz) was used to generate  
4 the frequency doubled  $\sim$ 308 nm (307.99 nm to excite the  $Q_1(2)$  rotational state) light for the  
5 fluorescence of OH radicals. Light was directed from the output of the laser and focussed into  
6 fibre optic cables (10 m, Oz Optics) which were then attached directly to the FAGE cell arms  
7 *via* collimators (Oz Optics). Fluctuations in laser power were accounted for using a linear  
8 response UV sensitive photodiode (UDT-555UV, Laser Components UK) at the exit arm of  
9 the OH and HO<sub>2</sub> detection axes to normalise the LIF signal. The laser system provided between  
10 5 – 7 and 2 – 3 mW of 308 nm light to the OH and HO<sub>2</sub> detection axes, respectively.

11 The OH fluorescence was collected orthogonal to the gas flow onto electronically gated  
12 Channeltron PhotoMultiplier tubes (CPM, Perkin Elmer, C943P) *via* a series of imaging lenses  
13 and a narrow bandpass filter (Barr Associates,  $308.8 \pm 5.0$  nm). A spherical concave back  
14 reflector was positioned underneath the cell, opposite the detection optics, to optimise light  
15 collection onto the CPM. To avoid detector saturation, the CPM was gated (i.e. switched off)  
16 for the duration of the laser pulse using a modified gating unit based on the original design by  
17 Creasey et al. (1997a). Signals from the CPM were analysed using PC-based photon counting  
18 cards (Becker and Hickl PMS-400A).

### 19 2.1.3 Other instrumentation

20 As with the previously published work (Winiberg et al., 2015), a chemiluminescence NO<sub>x</sub>  
21 analyser (TEC 42C, limit of detection = 50 pptv at 60 s averaging) was used to determine that  
22 levels of NO<sub>x</sub> (NO + NO<sub>2</sub>) in the HIRAC chamber were typically below the detection limit of  
23 the apparatus.

24 Most of the OH calibration experiments using the hydrocarbon decay method were  
25 performed monitoring HC decays using a chemical ionization time of flight mass spectrometer  
26 (Kore custom build) operating with N<sub>2</sub><sup>+</sup> ionization. Gas was sampled from HIRAC via  $\sim$ 7 m of  
27 1/8" Teflon tubing with the inlet being located close (within 70 cm) to the FAGE inlet. A  
28 majority of the experiments were carried out with cyclohexane as the HC (monitored at  $m/z =$   
29 84.15), although other compounds were used. The mass spectrometer signal was calibrated by  
30 introducing known HC concentrations into HIRAC. An example of the resulting calibration  
31 plot can be found in the SI (Section S2, Figure S3).

32

## 1 **2.2 General Chamber preparation**

2 Calibration experiments were conducted at 1000 mbar in an Ultra-High Purity (UHP) 1:4  
3 synthetic air mix of O<sub>2</sub> (BOC, zero-grade, >99.999%) and N<sub>2</sub> (BOC, zero-grade, >99.998%) to  
4 match the range of pressures from the water vapour calibration method (section 3.1). Thorough  
5 mixing of reaction mixtures within HIRAC was achieved in  $\leq 70$  s by four circulation fans  
6 mounted in pairs at each end of the chamber. The chamber was evacuated to  $\sim 0.05$  mbar for  
7  $\sim 60 - 120$  min following each experiment using the rotary pump backed roots blower to ensure  
8 removal of all reactants/products. The combined sampling rate of  $\sim 9$  slm from the chamber  
9 required a counter flow of synthetic air to maintain the desired pressure and resulted in a first  
10 order dilution term of  $(4.5 \pm 0.2) \times 10^{-5} \text{ s}^{-1}$ . The dilution flow was regulated using two Brooks  
11 mass flow controllers (N<sub>2</sub> and O<sub>2</sub>) and the dilution was taken in account in all analyses.

12

## 13 **2.3 Chemical reagents**

14 Known concentrations of precursors (except H<sub>2</sub>O<sub>2</sub>) and reagents were introduced to the  
15 chamber in the vapour phase through a 0.97 L stainless steel delivery vessel. Hydrogen  
16 peroxide (50% wt solution, Merck, used as supplied) was directly injected via a syringe.  
17 Multiple injections could be made in each run to ensure a wide range of [OH] was covered.

18 For the hydrocarbon based OH calibration method, cyclohexane (99%, Fischer Scientific),  
19 methylcyclohexane (>99.9%, Sigma Aldrich) and heptane (99%, Fischer Scientific) were  
20 purified using freeze-pump-thaw cycles before being introduced into the HIRAC chamber.

21 For the second-order HO<sub>2</sub> calibration method, formaldehyde (HCHO) was produced in the  
22 gas phase by gently heating paraformaldehyde (99.9%, Sigma Aldrich) into the evacuated  
23 delivery vessel. This method was sufficient for producing the 2 – 3 ppmv concentrations of  
24 HCHO in the HIRAC chamber that were required.

25

## 26 **3 Calibration methods**

### 27 **3.1 Flowtube/Water Photolysis Calibration Method**

28 The flowtube calibration method relies on the photolysis of H<sub>2</sub>O vapour at 184.9 nm in a fast  
29 flow (40 slm) of synthetic air. A mercury penray lamp (LOT-Oriel, Hg-Ar) was used as the  
30 photolysis source, placed at the end of a square cross section flow tube ( $12.7 \times 12.7 \times 300$  mm).  
31 Air was humidified by passing a fraction of the bulk air flow through a bubbler containing

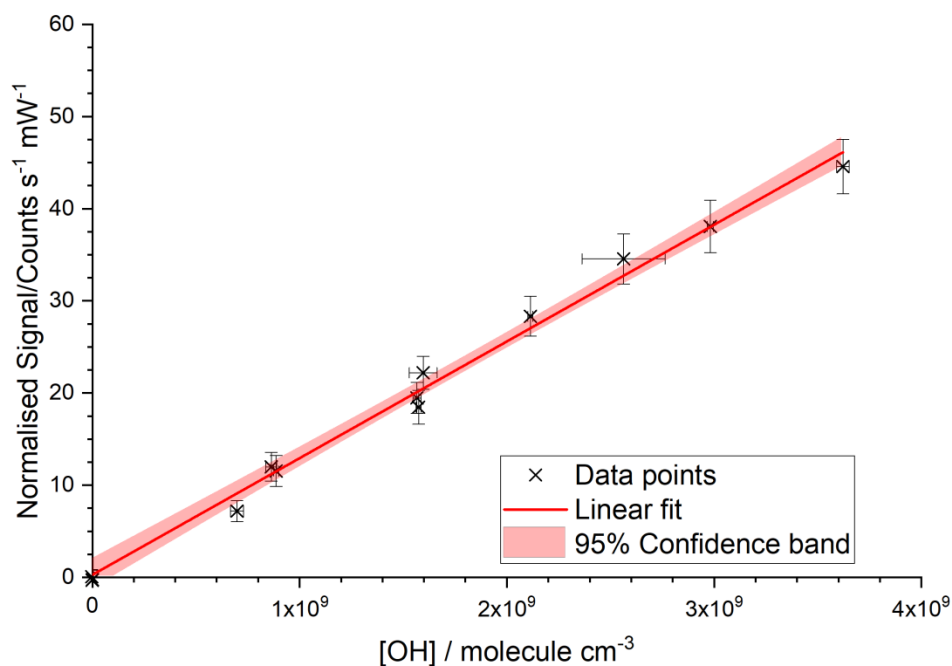


1 deionised water. The [H<sub>2</sub>O] was measured using a dew-point hygrometer (CR4, Buck Research  
2 Instrument) prior to the flow tube and the resulting OH and HO<sub>2</sub> concentrations from photolysis  
3 can be calculated from equation (E2):

$$4 \quad [\text{OH}] = [\text{HO}_2] = [\text{H}_2\text{O}] \sigma_{\text{H}_2\text{O}, 184.9 \text{ nm}} \Phi_{\text{OH}} F_{184.9 \text{ nm}} \Delta t \quad (\text{E2})$$

5 where  $\sigma_{\text{H}_2\text{O}, 184.9 \text{ nm}}$  is the known absorption cross-section of H<sub>2</sub>O vapour at 184.9 nm  
6 ( $(7.22 \pm 0.22) \times 10^{-20} \text{ cm}^2 \text{ molecule}^{-1}$  (Cantrell et al., 1997; Creasey et al., 2000; Hofzumahaus  
7 et al., 1997)),  $\Phi_{\text{OH}}$  (=  $\Phi_{\text{HO}_2} = 1$ ) is the photodissociation quantum yield of OH and HO<sub>2</sub> (Fuchs  
8 et al., 2011),  $F_{184.9 \text{ nm}}$  is the photon flux of 184.9 nm light and  $\Delta t$  is the exposure time of the air  
9 to the Hg lamp output. The exposure time of the air to the 184.9 nm light,  $\Delta t$ , was calculated  
10 as a function of the known velocity of the air and the cross section of the photolysis region.  
11 The product  $F_{184.9 \text{ nm}} \times \Delta t$  was determined for lamp supply currents between 0.2 and 3.0 mA  
12 using the N<sub>2</sub>O actinometry method described in detail in a number of publications (Edwards et  
13 al., 2003; Heard and Pilling, 2003; Faloon et al., 2004; Whalley et al., 2007; Glowacki et al.,  
14 2007).

15 The gas output from the flow tube was directed towards the FAGE sampling inlet, where  
16 the overflow of the FAGE sample volume from the flow tube stopped the impingement of  
17 ambient air. A range of HO<sub>x</sub> concentrations ( $10^8 - 10^{10} \text{ molecule cm}^{-3}$ ) were produced by  
18 changing the mercury lamp photon flux whilst keeping a constant [H<sub>2</sub>O] (typically 2000 - 3000  
19 ppmv). The average calculated [HO<sub>x</sub>] values are compared to their concurrent OH/HO<sub>2</sub> signals  
20 observed during the same time period, the linear regression of which gives the instrument  
21 sensitivity to OH/HO<sub>2</sub>. A typical calibration plot is shown in Figure 1. Potential systematic  
22 errors in the flowtube calibration method have been discussed previously (Winiberg et al. 2015)  
23 and are summarized for the current instrument in Table 4 and discussed further in the SI,  
24 Section S3, which also contains a schematic of the flowtube calibration apparatus (Figure S4).



1

2 **Figure 1:** Typical room temperature calibration plot from the conventional water photolysis, flow tube  
 3 method. The total flow rate was 40 slm, with  $[H_2O] = 1600$  ppmv, the laser power was 9.65 mW and  
 4 the OH cell was at a pressure of 2.6 Torr. Gradient =  $(1.266 \pm 0.034) \times 10^{-8}$  counts  $s^{-1}$   $mW^{-1}$   $cm^3$   
 5  $molecule^{-1}$ , intercept =  $0.28 \pm 0.74$  counts  $s^{-1}$   $mW^{-1}$ . Errors are  $2\sigma$ .

6

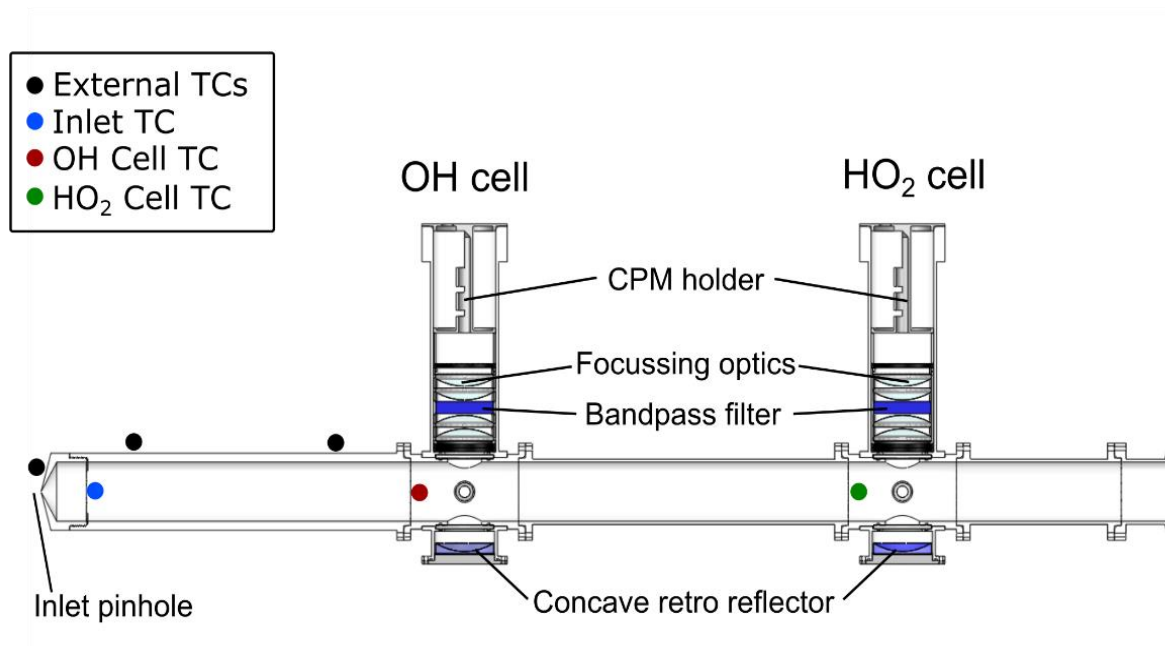
### 7 3.1.1 Calibration for External Inlet Temperature

8 The FAGE inlet was wrapped with  $\frac{1}{4}$ " copper tubing ( $\sim 5$  cm between coils) and covered in  
 9 two layers of aluminium foil to aid thermal contact. A final layer of 10 mm thick neoprene was  
 10 added to the outside of the foil to aid insulation. The Huber temperature control unit was used  
 11 to flow DW-THERM thermofluid through the tubing to vary the temperature of the inlet.  
 12 Temperatures were monitored externally using three K-type thermocouples; two positioned on  
 13 the inlet and one on the conical pinhole nozzle during the calibration procedure (see Figure  
 14 2(a)).

15 Calibrations were conducted at five external inlet temperatures from 263 – 343 K,  
 16 representative of the operating temperature range for the HIRAC chamber. During the bulk of  
 17 the experiments, gases from the flowtube calibration source were maintained at room  
 18 temperature. However, an additional range of calibration experiments were performed with  
 19 flowtube gas maintained to within  $\pm 5$  K of the measured external inlet temperature. This effect  
 20 was achieved by passing the humidified bulk flow through a 2 m long coil of  $\frac{1}{4}$ " copper tubing  
 21 held at the desired set point using a thermostat controlled water bath (Thermo Fischer Science).

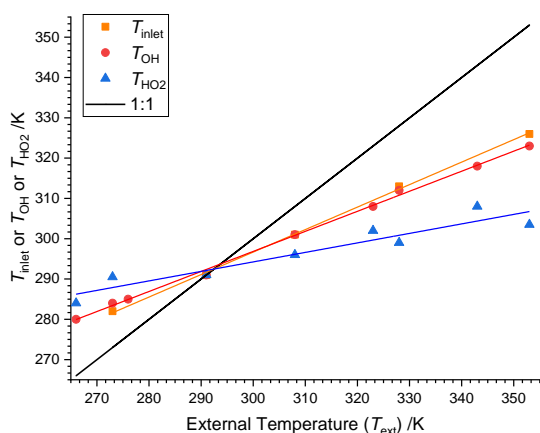
1 The  $[\text{H}_2\text{O}]_{\text{vap}}$  was determined just before the calibration flowtube, with the temperature  
 2 monitored both before and at the exit of the flowtube. Short gas lines were used between the  
 3 water bath and the flow tube, which was covered in a thin layer of neoprene to insulate and  
 4 reduce temperature gradients.

5 (a)

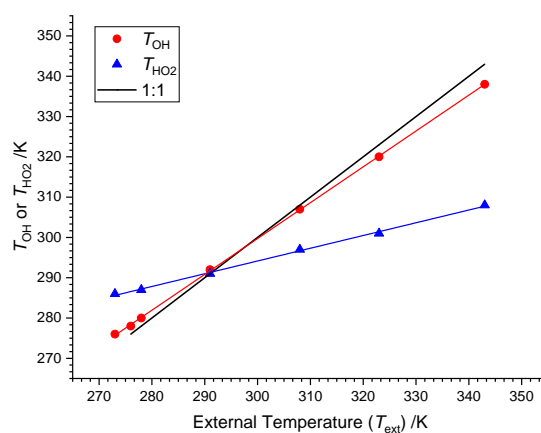


6

7 (b)



(c)



8 **Figure 2:** (a) Schematic of FAGE Cell showing locations of thermocouples. (b) Internal cell  
 9 temperatures ( $T_{\text{OH}}$  or  $T_{\text{HO}_2}$ ) and inlet temperatures ( $T_{\text{inlet}}$ ) plotted as a function of the external temperature  
 10 ( $T_{\text{ext}}$ ), when sampling air at 293 K from the calibration flowtube. Slope  $T_{\text{inlet}} = 0.558 \pm 0.010$ ; Slope  $T_{\text{OH}} = 0.497 \pm 0.008$ ;  
 11 Slope  $T_{\text{HO}_2} = 0.236 \pm 0.033$ . (c) Internal temperatures as a function of the external  
 12 temperature when sampling temperature controlled air from the calibration flowtube. Slope  $T_{\text{OH}} = 0.890 \pm 0.004$ ;  
 13 Slope  $T_{\text{HO}_2} = 0.316 \pm 0.007$  (sampling from the HIRAC chamber gave lines with essentially  
 14 the same gradients).

15

1

2 Prior to the calibration, the internal cell temperatures were measured using three K-type  
3 thermocouples positioned in the centre of the gas flow inside the inlet (just after the inlet  
4 pinhole), OH and HO<sub>2</sub> fluorescence cells, details of which are discussed in the results section  
5 (4.1.1). The thermocouples were inserted into the cell using a ¼” compression fitting port, seal;  
6 this allowed the cell to be operated at normal operating pressure during the temperature profile  
7 measurements. Thermocouples were held in place temporarily using electrical tape, and  
8 OH/HO<sub>2</sub> calibrations were not performed with the thermocouples in place.

9

### 10 **3.2 Hydrocarbon decay method**

11 A majority of the hydrocarbon decay OH measurements were made with cyclohexane as the  
12 monitored hydrocarbon (HC) (monitored via the  $m/z = 84.15$  peak) and hydrogen peroxide  
13 photolysis at 254 nm as the OH source.

14 The principle of the hydrocarbon decay method was outlined in the introduction; the rate of  
15 loss of the HC by OH is given by:

$$16 \quad -\frac{d[\text{HC}]}{dt} = k_{bi}[\text{OH}][\text{HC}] \quad (\text{E1})$$

17 The rate coefficient for cyclohexane, c-C<sub>6</sub>H<sub>12</sub>, has received much attention in the literature over  
18 the 273 – 343 K temperature range used in this study, and so we use the IUPAC recommended  
19 rate expression (Atkinson et al., 2006):

$$20 \quad k_{\text{OH}+\text{c-C}_6\text{H}_{12}} = 3.26 \times 10^{-17} T^2 e^{(262 \pm 66)/T} \text{ cm}^3 \text{ molecule}^{-1} \text{ s}^{-1} \quad (\text{E3})$$

21 The calculated [OH] from the hydrocarbon decay can be compared to the corresponding FAGE  
22 signal, corrected for the difference in [H<sub>2</sub>O] used in the calibration and that present in the  
23 HIRAC chamber, to determine the C<sub>OH</sub>. In practice, the total HC decay is a combination of  
24 reaction with OH and other first order loss processes, primarily dilution (as sampled gas is  
25 replenished with air). Therefore

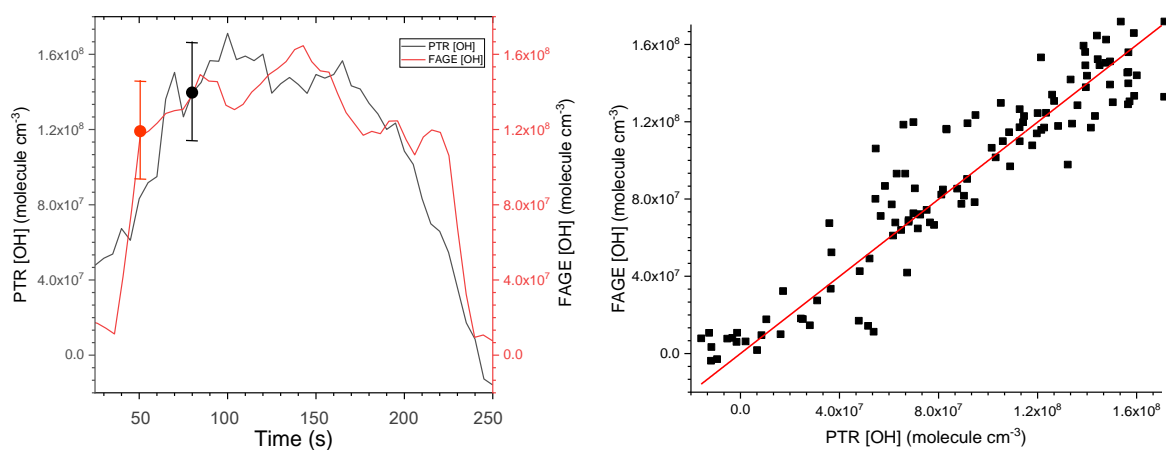
$$26 \quad -\frac{d[\text{HC}]}{dt} = k_{1st}[\text{HC}] + k_{bi}[\text{OH}][\text{HC}] \quad (\text{E4})$$

27 where  $k_{1st}$  represents the rate coefficient for the sum of all non-OH first order loss processes  
28 (e.g. heterogeneous loss and dilution). Gradients were obtained from analysis within the Origin  
29 software package. A second order polynomial was fitted to 10 – 40 points (with the separation

1 of each point being 10 s); the number of points depending on the rate of change of the [HC]  
2 and the data points were smoothed via the method of Savitzky and Golay (1964).

3  $k_{1st}$  was determined from the HC decays in the absence of OH (either with no lamps on, or  
4 no OH precursor present). For each injection of HC (typical initial concentration of  $3 - 5 \times$   
5  $10^{13}$  molecule  $\text{cm}^{-3}$ ) there were multiple  $\text{H}_2\text{O}_2$  injections ( $\sim 1$  ml). FAGE measurements were  
6 typically averaged over 30 s (30 data points, with each data point corresponding to accumulated  
7 signal over  $\sim 1$  s) to counteract the noise arising in fluorescence counts. During rapid changes  
8 in the observed signal, for example immediately after initial photolysis of hydrogen peroxide  
9 in the chamber (see Figure 3(a)), a reduced averaging period was used. The HIRAC FAGE  
10 system shows a slight sensitivity to water vapour concentrations due to quenching (Winiberg,  
11 2014). Minor corrections ( $<5\%$ ) were made to account for the different water vapour  
12 concentrations in the two calibration methods.

13 Figure 3(a) shows a typical time series of OH with the black line giving the [OH] derived  
14 from the mass spectrometer measurements and the brown line giving [OH] derived from the  
15 FAGE signal and converted to [OH] using the conventional flow tube water vapour photolysis  
16 calibration at 293 K. Figure 3(b) shows the resulting scatter plot. The slope of the scatter plot  
17 gives the correction to be applied to  $C_{293\text{ K}}$  from the conventional calibration to match the [OH]  
18 derived from the mass spectrometric measurements.

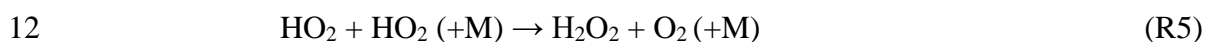


19 **Figure 3:** a) Time series of [OH] derived from FAGE measurements and from mass spectrometric  
20 measurements of cyclohexane removal recorded following  $\text{H}_2\text{O}_2$  photolysis at 293 K and 1000 mbar  
21 air. The error bars shown represent absolute uncertainties in the calibration methods, see Table 4. b)  
22 Resultant scatter plot where the gradient,  $0.998 \pm 0.016$  ( $2\sigma$ ) gives  $C_{rel}$  for the FAGE apparatus at 293  
23 K for this experiment. The average gradient at 293 K is  $1.034 \pm 0.0068$  from five experiments.

24

### 3.3 Calibration of HO<sub>2</sub> detection via HO<sub>2</sub> recombination kinetics

The HCHO photolysis/HO<sub>2</sub> recombination kinetics method of HO<sub>2</sub> cell calibration was used as described in Winiberg et al. (2015). Formaldehyde was introduced in a flow of nitrogen into the chamber (containing synthetic air at 1000 mbar) at concentrations of  $\sim 2 \times 10^{13}$  molecule cm<sup>-3</sup>. The chamber was irradiated (lamps: Philips TL40W/12 RS) resulting in an almost instantaneous HO<sub>2</sub> signal (reactions R2 – R4). Once a steady state HO<sub>2</sub> concentration was achieved, the photolysis lamps were turned off and the decay of HO<sub>2</sub> was monitored by FAGE for  $\sim 120$  s (Figure 4). The decay of HO<sub>2</sub> was primarily controlled by the self-reaction (R5), but there was a small first-order contribution from loss to the walls (R6). The measurement of HO<sub>2</sub> decays was repeated up to six times before the laser wavelength was scanned to the offline position.



The chamber mixing fans were used for the first three calibration decays, representative of a typical experimental homogeneous gas mixture. The second series of three calibration decays were conducted without the mixing fans to probe the HO<sub>2</sub> recombination and wall loss kinetics in the absence of effective mixing.

When the fans are on, the loss of HO<sub>2</sub> was characterised by bimolecular self-reactions and a first order wall loss parameter. The solution to this mixed order decay is given by:

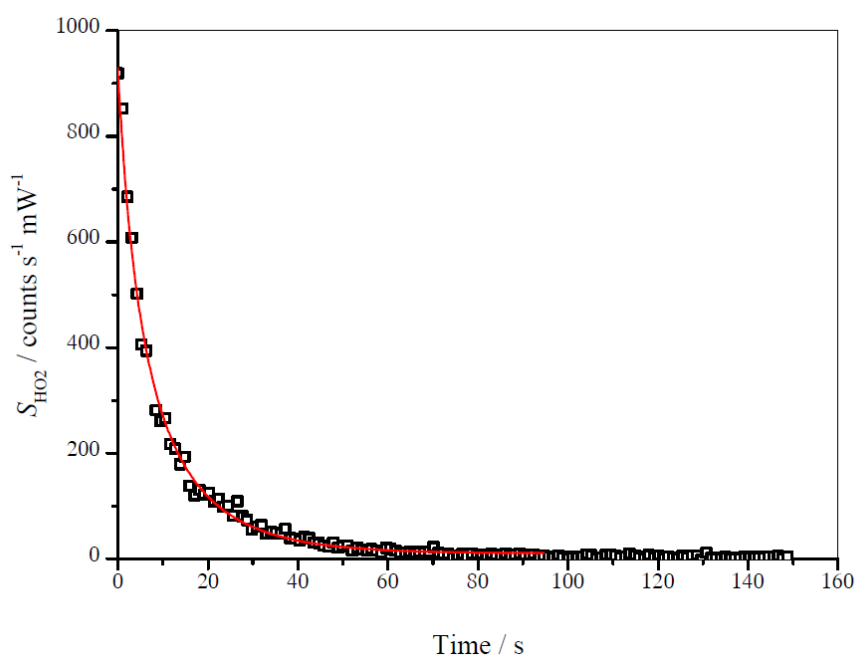
$$(S_{\text{HO}_2})_t = \left( \left( \frac{1}{(S_{\text{HO}_2})_0} + \frac{2 \cdot k_{\text{HO}_2+\text{HO}_2}}{k_{\text{loss}} \cdot C_{\text{HO}_2}} \right) \cdot e^{(k_{\text{loss}} t)} - \left( \frac{2 \cdot k_{\text{HO}_2+\text{HO}_2}}{k_{\text{loss}} \cdot C_{\text{HO}_2}} \right) \right)^{-1} \quad (\text{E5})$$

where  $(S_{\text{HO}_2})_t$  and  $(S_{\text{HO}_2})_0$  are the HO<sub>2</sub> signal at time  $t$  and  $t = 0$  respectively,  $(C_{\text{HO}_2})$  is the instrument sensitivity,  $k_{\text{HO}_2+\text{HO}_2}$  is the HO<sub>2</sub> recombination rate coefficient and  $k_{\text{loss}}$  represents the wall loss parameter. Both  $k_{\text{loss}}$  and  $C_{\text{HO}_2}$  were determined by data fitting the  $S_{\text{HO}_2}$  decay using equation (E5) with a Levenburg-Marquardt non-linear least squares algorithm, fixing the initial signal and  $k_{\text{HO}_2+\text{HO}_2}$ . The first  $\sim 100$  s of data were used, ensuring analysis after an almost complete decay of  $S_{\text{HO}_2}$ . Figure 4 shows an example of a typical decay and the resulting fit to equation (E5).

For the experimental temperature range (275 – 345 K),  $k_{\text{HO}_2+\text{HO}_2}$  has values between  $(2.00 - 2.85) \times 10^{-12}$  cm<sup>3</sup> molecule<sup>-1</sup> s<sup>-1</sup> according to the recommendation given by IUPAC

1 (2007). The chamber was operated under dry conditions ( $< 10$  ppmv  $[\text{H}_2\text{O}]_{\text{vap}}$ ), and so the  
2 enhancement of  $k_{\text{HO}_2+\text{HO}_2}$  by formation of a pre-reactive complex with  $\text{H}_2\text{O}$  was ignored for  
3 these analyses. The wall loss rate,  $k_{\text{loss}}$ , was dependent on daily chamber conditions and was  
4 therefore determined as part of the fitting procedure along with  $C_{\text{HO}_2}$ , typically between  
5  $0.032 - 0.073 \text{ s}^{-1}$  with an uncertainty of  $\pm 10\%$  ( $2\sigma$ ). Without the fans, the value of  $k_{\text{loss}}$  was  
6 reduced, but agreement between the  $\text{HO}_2$  calibration methods was comparable (within 10%).  
7 As HIRAC is generally operated with fans on, we have only reported these data. Wall loss  
8 typically contributes 10 – 50% of the initial decay but is well defined in the fitting procedure.  
9 As with OH detection, minor corrections have been made for the slightly different sensitivities  
10 of the system under the different water concentrations of the two calibration methods  
11 (Winiberg, 2014).

12



13

14 **Figure 4:** Typical  $\text{HO}_2$  decay recorded at 293 K and 1000 mbar air. The red line is the fit to  
15 the data from equation (E5) giving  $C_{\text{HO}_2, 293 \text{ K}} = (4.17 \pm 1.66) \times 10^{-8} \text{ counts cm}^3 \text{ molecule}^{-1}$   
16  $\text{mW}^{-1} \text{ s}^{-1}$

17

## 1 4 Results and Discussion

### 2 4.1 Conventional Calibration method

#### 3 4.1.1 Temperature profiles in the FAGE instrument

4 Temperatures within the FAGE instrument as a function of external temperatures are shown in  
5 Figures 2(b) and (c) and tabulated in Table 1. For Figure 2(b) and the first part of Table 1, the  
6 temperatures were recorded with FAGE sampling air at 293 K from the calibration flow tube  
7 as the FAGE inlet was cooled or heated. Temperatures became closer to ambient (293 K) from  
8 the inlet ( $T_{\text{inlet}}$ ) to the OH observation cell ( $T_{\text{OH}}$ ) and finally to the HO<sub>2</sub> observation cell ( $T_{\text{HO}_2}$ ).  
9 In Figure 2(c) and the second part of Table 1, the sampled air (either from the calibration flow  
10 tube or from HIRAC) matched the external temperature of the inlet tube. For these experiments,  
11 there was no thermocouple located inside the inlet to give  $T_{\text{inlet}}$ . The temperature in the OH cell  
12 was very close to the external temperature of the sampled air. The transmission process through  
13 the FAGE inlet following sampling through the pinhole should be similar to when FAGE is in  
14 HIRAC, however, even with the temperature controlled air in the wand calibration, it is still  
15 difficult to determine the actual temperature and conditions at the pinhole itself.

16 The gap between the OH and HO<sub>2</sub> cells means that the sampled air was closer to ambient  
17 room temperatures when reaching the HO<sub>2</sub> cell. HO<sub>2</sub> was predominantly exposed to a  
18 temperature environment similar to that for OH as it passed through the inlet, which may  
19 influence wall loss rates. The variation in  $T_{\text{OH}}$  and  $T_{\text{HO}_2}$  relative to room temperature under  
20 different calibration regimes means that care has to be taken in comparing  $C_{\text{HO}_x}$  values, as a  
21 number of processes within FAGE are temperature dependent. Nevertheless, the different  
22 calibration methods do yield important insights into the processes in the FAGE apparatus.

23

24



1 **Table 1:** Temperature Calibration of the FAGE instrument with a) constant temperature (293  
 2 K) calibration gas b) with calibration gas at the external temperature.

External Temperature/K ( $T_{\text{ext}}$ )	Inlet Temperature /K, ( $T_{\text{inlet}}$ )	OH FAGE Cell Temperature /K, ( $T_{\text{OH}}$ )	HO <sub>2</sub> FAGE Cell Temperature /K, ( $T_{\text{HO}_2}$ )
<i>Ambient Calibration Air at 293 K</i>			
266 <sup>a</sup>		280	284
273	282	284	290.5
276		285	
293	293	293	293
308	301	301	296
323		308	302
328	313	312	299
343		318	308
353	326	323	313.5
<i>Calibration Air Matched to FAGE Inlet Tube Temperature</i>			
273		276	286
276		278	
278		280	287
293		293	293
308		307	297
323		320	301
343		338	308

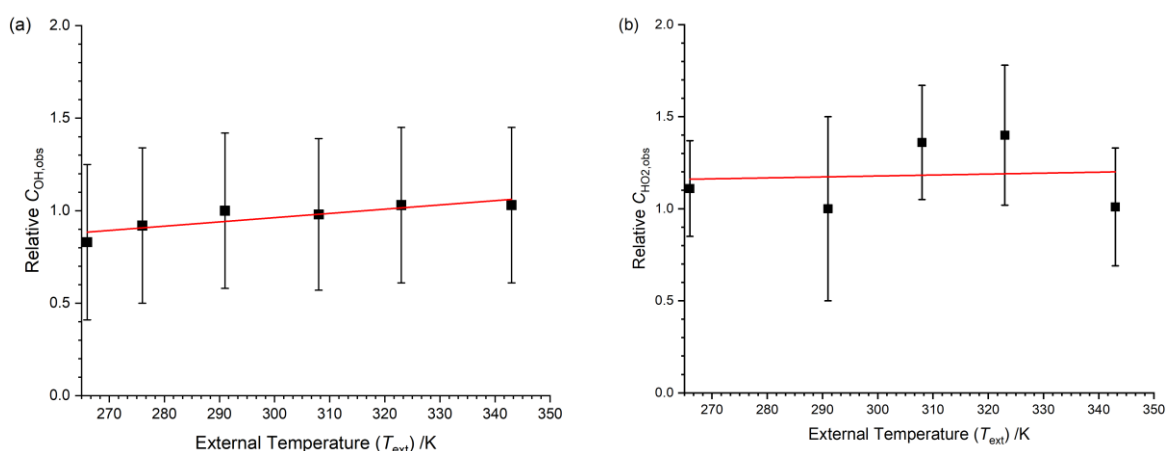
3 a – All temperature measurements have uncertainty of  $\pm 0.5$  K.

4 Figures 2(b) and (c) show the linear relationship between the internally measured  
 5 temperature at the pinhole, OH cell and HO<sub>2</sub> cell. For Figure 2(b), the linear regression of the  
 6 data gives ratios of  $0.556 \pm 0.002$ ,  $0.510 \pm 0.002$  and  $0.195 \pm 0.002$  for the inlet thermocouple  
 7 (close to the pinhole), OH cell and HO<sub>2</sub> cell. The temperature in the OH cell is controlled by  
 8 the external temperature. In contrast, in field instruments which have a very different design  
 9 and where OH is probed very close to the pinhole, there is a significant cooling effect due to  
 10 the expansion (Creasey et al., 1997b). This is lost in the HIRAC FAGE due to the long inlet  
 11 prior to probing the OH.

#### 12 4.1.2 Temperature Dependent Flow Tube Calibration with Air at 293 K

13 Figure 5 displays the relative  $C_{\text{OH}}$  and  $C_{\text{HO}_2}$  for the HIRAC FAGE instrument as a function of  
 14 external temperature between 266 – 343 K, with the data points listed in the top half of Table  
 15 2. In these experiments the FAGE inlet was cooled or warmed to give the external temperature  
 16 ( $T_{\text{ext}}$ ). The air from the calibration flow tube was at a constant 293 K and therefore the  
 17 temperature in the observation cells (OH or HO<sub>2</sub>) was varying compared to the inlet air. This

1 method of investigating the temperature dependence of  $C_{\text{HOx}}$  therefore operates under different  
 2 conditions from the subsequent methods (Sections 4.1.3 and 4.2). Data for  $C_{\text{HOx}}$  are presented  
 3 relative to the calibration factor at room temperature (293 K).



4 **Figure 5:** Temperature dependence of the calibration factors ( $C_{\text{HOx}}$ ) as a function of the external  
 5 temperature with HOx being delivered from the calibration flow tube at a constant temperature. Solid  
 6 lines are a weighted fit to the data. (a)  $C_{\text{OH,obs}}$ , slope =  $(0.0023 \pm 0.0007) \text{ K}^{-1}$ . (b)  $C_{\text{HO}_2,obs}$ , slope =  $(0.0005$   
 7  $\pm 0.0031) \text{ K}^{-1}$ . Errors are  $2\sigma$ .

8  
 9  $C_{\text{OH,obs}}$  shows a positive temperature dependence ( $0.0023 \pm 0.0007 \text{ K}^{-1}$ ), for  $C_{\text{HO}_2,obs}$ , the data  
 10 appear to be more scattered and no systematic trend is observable. The overall temperature  
 11 dependence of both HOx calibration factors are small compared to the overall uncertainty in  
 12 the calibration (40%); the relative calibration factor for OH changes by about 20% from 266 –  
 13 343 K. However, the error bars in Figure 5 represent the total error in the calibration, much of  
 14 which will be temperature independent. A full discussion on the temperature dependence of  
 15 the calibration factors is presented in Section 4.3.

16  
 17

1 **Table 2:** Instrument sensitivity to OH,  $C_{OH}$ , and HO<sub>2</sub>,  $C_{HO_2}$ , determined using the  
 2 conventional water vapour calibration method.

$T_{ext}/K$	$T_{OH} / K$	$T_{HO_2} / K$	$C_{OH,obs}$	$C_{HO_2,obs}$
<i>Ambient Calibration Air at 293 K</i>				
266	280	284	$0.83 \pm 0.42$	$1.11 \pm 0.26$
276	285	-	$0.92 \pm 0.42$	- <sup>a</sup>
293	293	293	$1.00 \pm 0.42$	$1.00 \pm 0.50$
308	301	297	$0.98 \pm 0.41$	$1.36 \pm 0.31$
323	308	302	$1.03 \pm 0.42$	$1.40 \pm 0.38$
343	318	308	$1.03 \pm 0.42$	$1.01 \pm 0.32$
<i>Calibration Air Matched to FAGE Inlet Temperature (<math>T_{in}</math>)</i>				
276	278	-	$1.06 \pm 0.39$	- <sup>a</sup>
278	280	287	$0.91 \pm 0.50$	$1.43 \pm 0.54$
293	293	293	$1.00 \pm 0.40$	$1.00 \pm 0.45$
323	320	301	$1.18 \pm 0.39$	$1.91 \pm 0.38$
343	338	-	$1.45 \pm 0.39$	- <sup>a</sup>

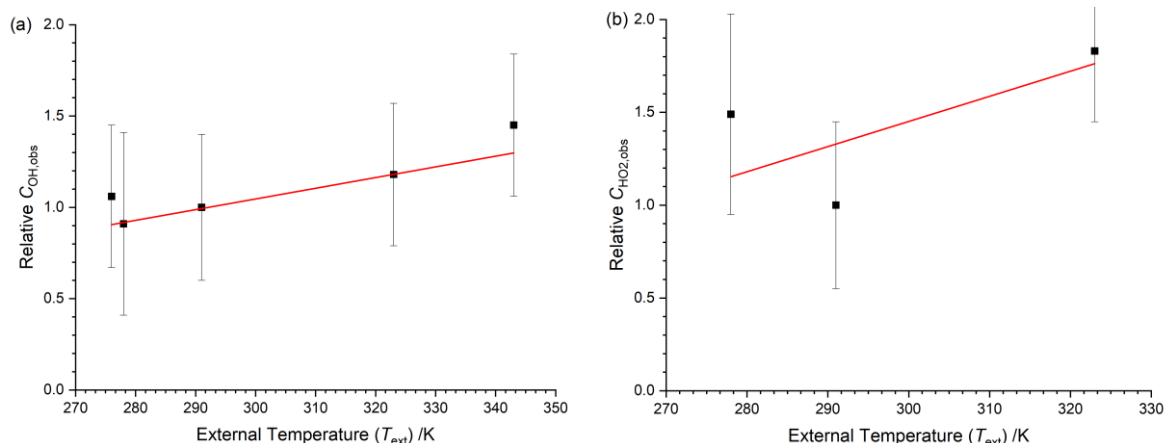
3 The internal temperatures ( $\pm 0.5$  K) for the OH and HO<sub>2</sub> fluorescence cells are represented by  $T_{OH}$  and  
 4  $T_{HO_2}$  respectively. a – determination of  $C_{HO_2}$  was precluded by a malfunctioning NO mass flow  
 5 controller.

6

### 7 4.1.3 Temperature Dependent Flow Tube Calibration with Air at Varying Inlet 8 Temperatures

9 A similar procedure to Section 4.1.2 was carried out, but in this case, the air flowing into the  
 10 calibration flow tube had been cooled/heated to match the external temperature of the FAGE  
 11 inlet. This method will give conditions that are more closely matched to those when the FAGE  
 12 instrument is located in the HIRAC chamber, where the FAGE inlet is at the same temperature  
 13 as the gas being sampled from HIRAC. The water vapour concentration was measured at a  
 14 fixed temperature in the dew-point hydrometer and therefore the [HO<sub>x</sub>] emitted from the wand  
 15 needed to be corrected for the change in [H<sub>2</sub>O] and additionally, for the change in  $\Delta t$  in equation  
 16 (E2).

17 In this calibration arrangement the temperature of the OH cell ( $T_{OH}$ ) was virtually identical  
 18 to the external temperature ( $T_{ext}$ ). The HO<sub>2</sub> FAGE cell was closer to ambient room temperature.  
 19 The temperature dependence of  $C_{HO_x,obs}$  relative to 293 K is shown in Figure 6. The calibrations  
 20 were taken at different times from those in Section 4.1.2, but the absolute  $C_{HO_x}$  factors at 293  
 21 K were in good agreement, within 5%. For OH, the slope of Figure 6(a) is again positive. For  
 22 HO<sub>2</sub> (Fig 6(b)) there are only three datum points and they are somewhat scattered.



1 **Figure 6:** Temperature dependence of the calibration factors ( $C_{HOx,obs}$ ) as a function of the external  
 2 temperature with HOx being delivered from the calibration flow tube at the external temperature. Solid  
 3 lines are a weighted fit to the data. (a)  $C_{OH,obs}$ , slope =  $(0.0059 \pm 0.0015) \text{ K}^{-1}$ . (b)  $C_{HO2,obs}$ , slope =  $(0.014$   
 4  $\pm 0.013) \text{ K}^{-1}$ .  
 5

## 6 4.2 Alternative Calibration Methods

### 7 4.2.1 Hydrocarbon Decay Calibration of OH Sensitivity

8 The ratio of the conventional water vapour flowtube calibration to the HC decay method  
 9 derived from scatter plots such as Figure 3 at 293 K was  $1.034 \pm 0.068$ , where the errors are  
 10 the statistical errors in the gradient of the scatter plots at the  $2\sigma$  level. The two methods are  
 11 therefore in excellent agreement as has been observed in our previous study conducted solely  
 12 at room temperature (Winiberg et al. (2015),  $1.19 \pm 0.26$ ). The increased number of data points  
 13 available for the HC analysis using PTR monitoring increases the precision of this work  
 14 compared to our earlier studies where [HC] was measured at much lower time resolution by  
 15 FTIR or gas chromatography.

16 A potential source of error in the HC decay method is quantifying the removal of the HC by  
 17 non-OH sources. The effects of dilution and wall loss can be accounted for by suitable blank  
 18 experiments, however, it is harder to account for any other chemically induced removal by  
 19 photolytically generated radicals other than OH in such blank experiments. The hydrocarbons  
 20 chosen for this analysis are simple alkanes with well-established chemistry that should  
 21 minimize such possibilities i.e., very slow reactions with any photolytically generated  $O_3$  or  
 22  $NO_3$ . In addition, when both cyclohexane (CH) and heptane (HEP) were used as the HC, the  
 23 gradient of the resulting relative rate plot ( $\ln([HEP]_0/[HEP]_t)$  vs  $\ln([CH]_0/[CH]_t)$ , slope =  $0.923$   
 24  $\pm 0.010$ ) was in good agreement the ratio of the literature rate coefficients for OH reactions

1 ( $k_{\text{HEP}}/k_{\text{CH}} = 0.97 \pm 0.14$  at 298 K (Atkinson, 2003)). This confirms that OH was the dominant  
 2 route for chemical removal (see SI, Section S4). A key assumption of the hydrocarbon decay  
 3 calibration method is that the OH is chemically removed by OH.

4

5 **Table 3:** Temperature Dependence of  $C_{\text{OH,obs}}$  Determined via the Hydrocarbon Decay Method

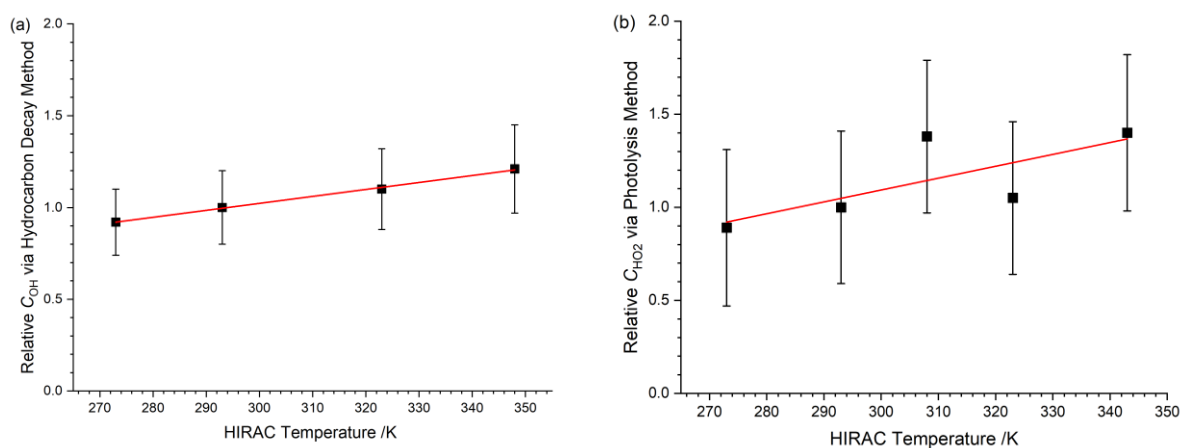
Temperature/K ( $\pm 0.5$ K)	$C_{\text{OH,obs}}$ relative to the HC decay method at 293 K
273	$0.92 \pm 0.17^{\text{a}}$
293	$1.00 \pm 0.18$
323	$1.10 \pm 0.20$
348	$1.21 \pm 0.22$

6

a – errors represent the total uncertainty in  $C_{\text{OH}}$ , see Table 4.

7

8 Displayed in Table 3 is the instrument sensitivity to OH radicals,  $C_{\text{OH,obs}}$ , measured between  
 9 273 and 348 K at 1000 mbar HIRAC chamber pressure using the hydrocarbon decay method  
 10 and Figure 7(a) shows these data as a function of the HIRAC temperature. An increase in  $C_{\text{OH}}$   
 11 is observed. As with the experiments carried out in Section 4.1.2, the temperature of the OH  
 12 cell ( $T_{\text{OH}}$ ) is very close to that of the gas being sampled at the inlet.



13 **Figure 7:** Temperature dependence of  $C_{\text{HO}_x,\text{obs}}$  relative to values at 293 K. Solid lines are a weighted fit  
 14 to the data. (a) Relative  $C_{\text{OH,obs}}$  from the HC decay method. Slope =  $(0.0038 \pm 0.0007) \text{ K}^{-1}$  (b) Relative  
 15  $C_{\text{HO}_2,\text{obs}}$  from the HCHO photolysis method. Slope =  $(0.0064 \pm 0.0034) \text{ K}^{-1}$ . Errors are  $2\sigma$ .

16

1 **Table 4:** The systematic uncertainties in the various parameters that determine the accuracy in  
 2 the OH and HO<sub>2</sub> calibration factors for the conventional and alternative calibration methods.

Conventional Flowtube		Hydrocarbon Decay		HCHO + <i>hν</i>	
Parameter	Uncertainty	Parameter	Uncertainty	Parameter	Uncertainty
$F_{184.9\text{ nm}} \times t$	20% <sup>a</sup>	$k_{\text{OH} - \text{c-C}_6\text{H}_{12}}$	12% <sup>b</sup>	$k_{\text{HO}_2 + \text{HO}_2}$	38% <sup>f</sup>
[H <sub>2</sub> O]	1%	$k_{\text{Dil}}$	2% <sup>c</sup>	$S_{\text{HO}_2}$ initial	10% <sup>g</sup>
$\sigma_{\text{H}_2\text{O}}$	3%	[c-C <sub>6</sub> H <sub>12</sub> ]	5%	Laser power	6%
Laser power	6%	Gradient	10%	Online Position	4% <sup>c</sup>
Online Position	4% <sup>c</sup>	Laser power	6%		
		Online Position	4% <sup>d</sup>		
<b>Error</b>	<b>22%<sup>e</sup></b>	<b>Error</b>	<b>18%<sup>e</sup></b>	<b>Error</b>	<b>40%<sup>e</sup></b>

3 a – Where the error is statistical, it is reported at the 1σ level.

4 b – Error estimated from literature review. Five recent determinations (NIST Kinetics) of the 298 K rate coefficient  
 5 give ~5% spread, added some additional uncertainty to account for temperature dependence.

6 c – Dilution determined from flow controller measurements.

7 d – The online position error is the approximate error in the maximum line intensity that is achieved when  
 8 positioning the laser wavelength at the centre of the OH transition.

9 e – Total accuracy is taken as the sum in quadrature of the individual uncertainties.

10 f – Error in rate coefficient from the IUPAC evaluation.

11 g – Uncertainties in the fitting parameters.

12

13 Table 4 summarizes the errors associated with the alternative calibration methods. For the  
 14 hydrocarbon decay method, the major uncertainties are in the rate coefficient of the  
 15 hydrocarbon (~12% for OH + cyclohexane), determination of cyclohexane concentration (5%)  
 16 and the gradient of the cyclohexane decay (10%). Other uncertainties are drifts in the laser  
 17 power (~6%, determined from monitoring a photodiode) and wavelength position (~4%).

#### 18 4.2.2 Calibration via HO<sub>2</sub> recombination kinetics

19 Displayed in Table 5 is the instrument sensitivity to HO<sub>2</sub>,  $C_{\text{HO}_2, \text{obs}}$ , determined using the  
 20 alternative calibration method between 273 and 343 K at 1000 mbar chamber pressure. Figure  
 21 7(b) shows  $C_{\text{HO}_2}$  as a function of temperature relative to the instrument sensitivity at 293 K.  
 22 Each measurement point represents the weighted average of at least five experimental data sets  
 23 and the error bars represent the total uncertainty in the instrument sensitivity to ±2σ. As with  
 24 the hydrocarbon decay method, the overall uncertainty is calculated as the sum in quadrature  
 25 of fit precision to the decay and the systematic uncertainties listed in Table 4. The largest  
 26 uncertainty was in the HO<sub>2</sub> self-reaction rate coefficient, dependent on the temperature used

1 (38%). The slope of the linear fit to the  $C_{\text{HO}_2}$  values is  $(0.0064 \pm 0.0034) \text{ K}^{-1}$ . The absolute  
 2 agreement between the conventional and HCHO photolysis methods at 293 K is good with  
 3  $C_{\text{HO}_2, \text{conventional}} = (3.38 \pm 1.08) \times 10^{-8} \text{ counts cm}^3 \text{ molecule}^{-1} \text{ mW}^{-1} \text{ s}^{-1}$  and  $C_{\text{HO}_2, \text{HCHO photolysis}} =$   
 4  $(3.69 \pm 1.48) \times 10^{-8} \text{ counts cm}^3 \text{ molecule}^{-1} \text{ mW}^{-1} \text{ s}^{-1}$ .

5

6 **Table 5:** Instrument sensitivity to  $\text{HO}_2$ ,  $C_{\text{HO}_2}$ , determined using the HCHO photolysis method  
 7 over the 273 – 343 K external inlet temperature range.

$T_{\text{HIRAC}} / \text{K}^{\text{a}}$	$T_{\text{HO}_2} / \text{K}^{\text{a}}$	$C_{\text{HO}_2} \text{ (rel. 293 K)}^{\text{b}}$
273	286	$0.89 \pm 0.36^{\text{c}}$
293	293	$1.00 \pm 0.40$
308	297	$1.38 \pm 0.55$
323	302	$1.05 \pm 0.42$
343	308	$1.40 \pm 0.56$

8

a – Error in temperature  $\pm 0.5 \text{ K}$ .

9

b – Values are relative to  $C_{\text{HO}_2, 293 \text{ K}}$  of  $(3.69 \pm 1.48) \times 10^{-8} \text{ counts cm}^3$   
 10  $\text{molecule}^{-1} \text{ mW}^{-1} \text{ s}^{-1}$ .

11

c – Each  $C_{\text{HO}_2}$  represents the weighted average of at least 5 individual  
 12 determinations. All experiments were conducted in 1000 mbar synthetic  
 13 air mixture.

12

13

14

14

## 15 4.3 Discussion of calibration methods and temperature dependence

### 16 4.3.1 Comparison of calibration methods

17 For room temperature, there is excellent agreement between the wand calibration and that for  
 18 OH based on hydrocarbon decays ( $[\text{OH}]_{\text{wand}}:[\text{OH}]_{\text{HC}} = 1.00:0.97$ ) and  $\text{HO}_2$  based on HCHO  
 19 photolysis and the kinetics of the  $\text{HO}_2$  recombination reaction ( $[\text{HO}_2]_{\text{wand}}:[\text{HO}_2]_{\text{kinetics}} =$   
 20  $1.00:1.09$ ). This is consistent with our earlier study (Winiberg et al. 2015) and has also been  
 21 confirmed in an intercomparison in the HIRAC chamber of the FAGE and NIR – CRDS (near  
 22 infrared cavity ring down spectroscopy) for  $\text{HO}_2$  (Onel et al., 2017a) and  $\text{CH}_3\text{O}_2$  (Onel et al.,  
 23 2020;Onel et al., 2017b).

24 For the hydrocarbon decay method there are several advantages compared to the  
 25 conventional wand calibration:

26 1) The  $[\text{OH}]$  is much closer to the conditions typically used in a chamber experiment ( $10^6 -$   
 27  $10^8 \text{ molecule cm}^{-3}$ ) whereas the lowest  $[\text{OH}]$  used in the wand calibration performed here is  
 28 typically  $10^8 \text{ molecule cm}^{-3}$ . Ideally one should calibrate over the same range as used in an  
 29 experiment.

- 1 2) This work has shown that there is a temperature dependence to the calibration factors.  
2 Calibrating via the hydrocarbon decay method provides identical conditions (temperature  
3 and pressure) to that of a real experiment in the HIRAC chamber. Temperature variation  
4 can be simulated using the conventional wand device, but this introduces additional  
5 uncertainty.
- 6 3) Conventional calibrations always take place with a significant water concentration, whereas  
7 the water concentration in the hydrocarbon decay can be set at any value.
- 8 4) Calibration can be achieved without removing the FAGE apparatus from the HIRAC  
9 chamber decreasing the time taken for calibration.

10 There are some disadvantages too. The calibration for OH is strongly dependent on the  
11 accuracy of the HC rate coefficient. It is therefore important to use a hydrocarbon with a well-  
12 characterised rate coefficient; realistically, even the best-characterised rate coefficient is likely  
13 to have an uncertainty of 5 – 10%. Several HC can be used to give multiple independent  
14 determinations of  $[\text{OH}]_{\text{HC}}$ , but this may increase the complexity of the analysis (e.g. coincident  
15 mass spectral peaks, or overlapping FTIR spectra) and reduce the absolute concentration of  
16 OH. Determination of  $[\text{OH}]_{\text{HC}}$  also relies on an accurate and precise determination of the  
17 concentration gradient and the  $[\text{HC}]$  at that time. PTR measurements provide a near continuous  
18 output, but if the  $[\text{HC}]$  is measured using systems with lower sampling rates (e.g. FTIR or GC),  
19 there can be a significant loss in precision of the gradient measurement.

20 Many of the advantages and disadvantages of the hydrocarbon decay method also apply to  
21  $\text{HO}_2$  kinetics method for  $\text{HO}_2$  calibration. The rate coefficient for  $\text{HO}_2$  recombination has a  
22 higher degree of uncertainty than many OH + hydrocarbon rate coefficients and is dependent  
23 on the amount of water present. In the HIRAC chamber the humidity can be kept very low, but  
24 that may not be possible in all chambers; in these circumstances the humidity would need to  
25 be measured and the rate coefficient adjusted.

26 All calibration methods are subject to systematic uncertainties, the magnitude of which may  
27 vary with conditions and therefore it is sensible to use a range of calibration methods.

#### 28 4.3.2 Temperature dependence of $C_{\text{HO}_x}$

29 Table 6 compares the relative observed  $C_{\text{HO}_x, \text{obs}}$  calibration factors for the three different  
30 calibration methods. In all cases, a positive temperature dependence is observed, but for  $C_{\text{HO}_2}$ ,  
31 only the alternative calibration method displays a statistically significant positive slope.



1 The  $C_{\text{HOx}}$  factors can be broken down into temperature independent components (laser  
2 power, solid angle of fluorescence collection, detector efficiency etc) and temperature  
3 dependent terms. Four temperature dependent terms are relevant for  $C_{\text{HOx}}$ : the number density  
4 of OH in the cell, the quenching efficiency of the fluorescence, the population of the probed  
5 quantum state of OH and the transmission efficiency through the pinhole and inlet tube  
6 (Creasey et al., 1997b). The first three terms can be calculated and hence accounted for. Any  
7 residual temperature dependence of  $C_{\text{HOx}}$  should then relate to the transmission coefficient  
8 through the apparatus.

9 *HOx number density* – The calculated [HOx] delivered to the FAGE apparatus depends on the  
10 temperature of the HOx source, either the wand (operating at a fixed  $T = 293$  K (Method 1) or  
11 at  $T_{\text{ext}}$  (Method 2) or the HIRAC chamber. If the temperature of the HOx cells are different  
12 from this temperature, then there will be a change in the number density of HOx, over and  
13 above that caused by the pressure changes between the HOx source (1 bar) and the HOx cell  
14 (typically 3.6 mbar). As the temperatures of the HOx cells have been measured it is  
15 straightforward to correct for the different number density in the observation cells and the  
16 resulting contribution to the temperature dependence of  $C_{\text{HOx}}$  as summarized in Tables S2-4.

17 *Quenching* – As shown in Faloon et al. (2004), the quenching parameter,  $Q(T)$ , is defined by  
18 integrating the OH fluorescence decay over the defined sample time, or gated region. The  
19 quenching rate coefficients for  $\text{N}_2$ ,  $\text{O}_2$  and  $\text{H}_2\text{O}$  have been shown to be dependent on  
20 temperature (Copeland and Crosley (1986) and (Bailey et al., 1997) for  $\text{N}_2$  and  $\text{O}_2$ , and Bailey  
21 et al. (1999) for  $\text{H}_2\text{O}$ ). The total decay intensity is defined by:  $[\text{OH}(\text{A}^2\Sigma^+, v' = 0)]_0 \exp(-\Gamma t)$ ,  
22 where  $\Gamma$ , the total OH lifetime, is defined approximately as the sum total of the radiative  
23 lifetime for OH,  $\gamma$ , and the non-radiative lifetime due to quenching by the aforementioned bath  
24 gases. Bailey et al. (1997) have calculated the impact of temperature on quenching accounting  
25 for both the change in the quenching rate coefficients and the change in the number density of  
26 the quenchers. Both the rate coefficient for quenching and the quencher number density  
27 decrease with increasing temperature and hence quenching overall decreases with increasing  
28 temperature (summarized in Table S5), enhancing the fluorescence quantum yield.

29 *Rotational population* – The rotational population of the probed state in the  $\text{Q}_1(2)$  transition  
30 will vary with temperature. The  $\text{Q}_1(2)$  is the transition giving the largest signal between 280 –  
31 340 K, the limits of  $T_{\text{OH}}$  explored in the study. Relative to ambient temperature, the rotational  
32 population probed by  $\text{Q}_1(2)$  increases by 3.5% at 280 K and decreases by 9.0% at the highest  
33  $T_{\text{OH}}$  of 340 K (Table S6).

1 It is therefore possible to calculate the expected variation in  $C_{\text{HO}_x}$  for the different calibration  
2 methods dependent on OH number density, quenching and rotational population; these can be  
3 compared with the observed variation in  $C_{\text{HO}_x}$  summarized in Table 6. Full details on the  
4 temperature dependences of the above components, which vary slightly with the calibration  
5 method used are presented in Section S5 of the SI.

6 The difference between the observed  $C_{\text{HO}_x}$  and the calculated  $C_{\text{HO}_x}$  due to the above  
7 parameters is attributed to increased transmission of HO<sub>x</sub> through the pinhole and inlet tube  
8 and is given in Table 6. The HO<sub>x</sub> transmission, to the fluorescence region will depend on the  
9 magnitude of heterogeneous loss of radicals to the walls of the FAGE inlet. The wall loss  
10 process is a combination of diffusion and uptake at the wall and the actual temperature  
11 dependence will depend on the radical, conditions and wall composition (Howard, 1979).

12 For the OH calibrations, there is an increase in OH transmission with temperature across all  
13 three calibration methods, consistent with a decrease in OH loss to the walls which has been  
14 observed in previous flow tube studies. OH wall loss rate in the inlet tube is usually  
15 approximated to a first order process with a rate coefficient,  $k_w$ , and decreasing values of  $k_w$   
16 with temperature have been reported for flow tube studies of OH reactions (Howard, 1979), for  
17 example Brown et al. (1990) report  $k_w$  decreasing from 35 s<sup>-1</sup> at 227 K to 5 s<sup>-1</sup> at room  
18 temperature.

19 For HO<sub>2</sub> measurements, there is potentially a further temperature dependent component, the  
20 conversion of HO<sub>2</sub> into OH via R7:



22 The rate coefficient for this reaction has a negative temperature dependence and the increased  
23 number density of NO would further enhance the rate of reaction at lower temperatures. The  
24 experiments reported in this work operated with excess NO such that the small variations in  
25 the rate of reaction over the range of  $T_{\text{HO}_2}$  (284 – 313 K) will not alter the conversion of HO<sub>2</sub>  
26 to OH. However, if one were working at lower HO<sub>2</sub> conversions to mitigate against RO<sub>2</sub> to OH  
27 conversion (Whalley et al. 2013), then variations in the conversion efficiency could change  
28  $C_{\text{HO}_2}$  as a function of temperature.

29 Temperature dependent HO<sub>2</sub> calibrations based on the conventional wand method give  
30 significant scatter, but a positive increase in HO<sub>2</sub> transmission is observed for the alternative  
31 calibration method based on HO<sub>2</sub> kinetics, the magnitude of which is similar to that for OH,  
32 albeit with significant error bars. In general, HO<sub>2</sub> and RO<sub>2</sub> radicals exhibit lower wall loss rate

**Table 6:** Summary of the temperature dependence of  $C_{HO_x}$  with different calibration methods

Method	Observed slope of relative $C_{OH,obs}$ with temperature	Calculated contribution <sup>a</sup>	Difference (relative OH transmission)	Observed slope of relative $C_{HO_2,obs}$ with temperature	Calculated contribution <sup>a</sup>	Difference (relative $HO_2$ transmission)
Heated FAGE inlet, ambient air at 293 K	$(0.0023 \pm 0.0007) K^{-1}$	$(0.0001 \pm 0.0010) K^{-1}$	$(0.0022 \pm 0.0012) K^{-1}$	$(0.0005 \pm 0.0031) K^{-1}$	$(0.0000 \pm 0.0010) K^{-1}$	$(0.0000 \pm 0.0032) K^{-1}$
Heated FAGE inlet, match air	$(0.0059 \pm 0.0015) K^{-1}$	$(0.0029 \pm 0.0010) K^{-1}$	$(0.0030 \pm 0.0018) K^{-1}$	$(0.014 \pm 0.013) K^{-1}$	$(0.0033 \pm 0.0010) K^{-1}$	$(0.0029 \pm 0.0016) K^{-1}$
Alternative kinetics based methods	$(0.0038 \pm 0.0007) K^{-1}$	$(0.0027 \pm 0.0010) K^{-1}$	$(0.0011 \pm 0.0012) K^{-1}$	$(0.0064 \pm 0.0034) K^{-1}$	$(0.0032 \pm 0.0010) K^{-1}$	$(0.0032 \pm 0.0035) K^{-1}$

a - Contribution from the change in number density, quenching and relative rotation population in the probed state.

1 coefficients, but in our FAGE system, HO<sub>2</sub> molecules have to travel further to reach the  
2 titration region where reaction occurs with NO to convert HO<sub>2</sub> to OH. Therefore, there is also  
3 potential for OH loss from the titration point to the second detection cell.

#### 4 4.3.3 Comparison with other instruments

5 The temperature dependence of the calibration factors will be strongly dependent on the design  
6 of the FAGE apparatus. Our instrument was designed with a long (~ 1 m) inlet such that we  
7 can probe across the diameter of the HIRAC chamber to check for radial distributions of  
8 radicals (Malkin et al., 2010). Hence, we would expect HO<sub>x</sub> transmission to play a significant  
9 role in the temperature dependence of the calibration factor which is observed. Any similarly  
10 designed instrument would have a contribution from HO<sub>x</sub> transmission, the magnitude of  
11 which would depend on inlet length/residence time and construction material. Heating the inlet  
12 should reduce transmission losses. The aircraft based instrument, from the Juelich research  
13 group, uses a PID controlled heater to maintain their FAGE inlet at ~300 K, mitigating any  
14 possible temperature effects. They have an in-field calibration system, also, which has shown  
15 negligible deviation from the expected behaviour at 300 K, based on the sample gas altitude  
16 temperature (Marno et al., 2020).

17 Regelin et al. (2013) have reported a similar temperature dependence study of C<sub>OH</sub> and C<sub>HO<sub>2</sub></sub>  
18 as the current flowtube study with the aircraft based HORUS instrument. Cooling lines were  
19 wound around the inlet to simulate the measured temperature profile and ambient air was  
20 sampled from a calibration flow tube. In contrast to our slight increase in C<sub>OH</sub> with temperature  
21 in the flow tube experiment, Regelin et al. observed a slight negative dependence of the OH  
22 signal. Regelin et al. report that their calculations have shown that the sample forms a jet  
23 between the pinhole and the OH cell such that there is insignificant interaction with the walls  
24 and therefore transmission will not be a problem.

25 In contrast, a significant decrease in HO<sub>2</sub> signal, S<sub>HO<sub>2</sub></sub>, (50%) was observed as the  
26 temperature was decreased from ~295 to ~262 K (slope = 0.017 K<sup>-1</sup> normalised to S<sub>HO<sub>2</sub>,293 K</sub>),  
27 i.e. the same qualitative behaviour as we observed, approximately a factor two greater than  
28 measured in our work, based on HO<sub>2</sub> recombination kinetics. Beyond the OH cell in the  
29 HORUS experiment, the jet breaks up and Regelin et al. suggest that temperature dependent  
30 wall losses are responsible for the change in S<sub>HO<sub>2</sub></sub>. Quantitative comparisons cannot be made  
31 due to the differences in construction. The observed temperature dependence of C<sub>OH</sub> and C<sub>HO<sub>2</sub></sub>

1 for the HORUS and HIRAC experiments emphasise the important of performing calibrations  
2 for each instrument under conditions as close as possible to those used in measurements.

### 3 **5 Conclusions**

4 The effect of temperature of the incoming sample on the sensitivity of the HIRAC FAGE  
5 instrument to OH and HO<sub>2</sub> has been investigated between 266 and 348 K using a combination  
6 of conventional water vapour photolysis/flow tube method (Faloona et al.) and alternative  
7 calibration methods based on hydrocarbon decays for OH and the HO<sub>2</sub> self-reaction for HO<sub>2</sub>.  
8 In all cases, a positive increase in sensitivity was observed (Table 6) although with large error  
9 bars in the case of HO<sub>2</sub> with conventional calibration.

10 The temperature dependence of the calibration factor can be broken down to four  
11 components. Variations in three parameters: number density, quenching and rotational  
12 population of the probed level, can be accounted for if the temperature and pressure in the LIF  
13 cells are monitored. The difference between the observed and calculated temperature  
14 dependence for the above parameters, has been attributed to HO<sub>x</sub> transmission from the pinhole  
15 to the relevant detection chamber.

16 The temperature dependence of  $C_{\text{HO}_x}$  will depend on the design and construction materials  
17 of the FAGE apparatus. It is therefore difficult to utilise the results of this study to predict  
18 results in other systems. However, for any systems with significant sampling inlet residence  
19 times, such as the HIRAC FAGE described in this work, increased HO<sub>x</sub> transmission with  
20 increasing temperature should be expected. Therefore, maintaining the inlet at a relatively high  
21 temperature should improve sensitivity in low temperature applications.

22 The *in situ* calibration methods (hydrocarbon decay and HO<sub>2</sub> recombination kinetics) offer  
23 important advantages in that the FAGE apparatus is calibrated under the physical conditions  
24 and [HO<sub>x</sub>] that more closely correspond to real experiments. All calibration methods are  
25 subject to significant uncertainty, however, the origins of these uncertainties are different and  
26 hence good agreement between calibration methods should provide confidence that significant  
27 systematic errors are not present.

28

### 29 **Supplementary Information**

30 Supplementary information; HIRAC temperature profiles, calibrations, further discussions on  
31 calibration uncertainties, relative rate plots to confirm OH as the key species in hydrocarbon

1 removal and further discussion on the temperature dependence of the FAGE signal can be  
2 found at \*\*\*\*\*.

3

#### 4 **Code/Data availability**

5 Any raw data is available either in the Supplementary Information or via contacting Prof. Paul  
6 Seakins.

7

#### 8 **Author Contributions**

9 FAFW and IGB led the initial work on OH temperature dependence performing all experiments  
10 with external calibration, WJW, THS and GB completed the experiments with HC decays in  
11 HIRAC, CAB and IGB completed experiments on HO<sub>2</sub> temperature dependence. PWS, DEH  
12 and DS planned and supervised the experiments and wrote the manuscript with contributions  
13 from all co-authors.

14

#### 15 **Competing Interests**

16 DEH is a member of the editorial board of AMT, otherwise the authors declare that they have  
17 no conflict of interest.

18

#### 19 **Acknowledgements**

20 The authors would like to thank NERC for studentships for FAFW and WJW. CAB was  
21 sponsored by a studentship from EPSRC. GB was supported by NERC grant NE/S010246/1,  
22 IB by the Marie Curie Fellowship LAMUNIO (no. 302342) and THS by the EU funded  
23 EUROCHAMP2020 project.

24

#### 25 **References**

26 Atkinson, R.: Kinetics of the gas-phase reactions of OH radicals with alkanes and cycloalkanes,  
27 Atmos. Chem. Phys., 3, 2233-2307, 10.5194/acp-3-2233-2003, 2003.

28 Atkinson, R., Baulch, D. L., Cox, R. A., Crowley, J. N., Hampson, R. F., Hynes, R. G., Jenkin,  
29 M. E., Rossi, M. J., and Troe, J.: Evaluated kinetic and photochemical data for atmospheric  
30 chemistry: Volume II - gas phase reactions of organic species, Atmospheric Chemistry and  
31 Physics, 6, 3625-4055, 2006.

- 1 Bailey, A. E., Heard, D. E., Paul, P. H., and Pilling, M. J.: Collisional Quenching of OH by N<sub>2</sub>,  
2 O<sub>2</sub> and CO<sub>2</sub>, *Journal of the Chemical Society, Faraday Transactions*, 93, 2915-2920, 1997.
- 3 Bailey, A. E., Heard, D. E., Henderson, D. A., and Paul, P. H.: Collisional quenching of  
4 OH(A<sup>2</sup>Σ<sup>+</sup>, v'=0) by H<sub>2</sub>O between 211 and 294 K and the development of a unified model for  
5 quenching, *Chem. Phys. Lett.*, 302, 132-138, 1999.
- 6 Bejan, I. G., Winiberg, F. A. F., Mortimer, N., Medeiros, D. J., Brumby, C. A., Orr, S. C.,  
7 Kelly, J., and Seakins, P. W.: Gas-phase rate coefficients for a series of alkyl cyclohexanes  
8 with OH radicals and Cl atoms, *International Journal of Chemical Kinetics*, 50, 544-555,  
9 10.1002/kin.21179, 2018.
- 10 Brown, A. C., Canosamas, C. E., Parr, A. D., and Wayne, R. P.: Laboratory studies of some  
11 halogenated ethanes and ethers - measurements of rates of reaction with OH and of infrared-  
12 absorption cross-sections, *Atmospheric Environment Part a-General Topics*, 24, 2499-2511,  
13 10.1016/0960-1686(90)90341-j, 1990.
- 14 Cantrell, C. A., Tyndall, G., and Zimmer, A.: Absorption cross sections for water vapour from  
15 183 to 193 nm, *Geophysical Research Letters*, 24, 2195-2198, 1997.
- 16 Commane, R., Floquet, C. F. A., Ingham, T., Stone, D., Evans, M. J., and Heard, D. E.:  
17 Observations of OH and HO<sub>2</sub> radicals over West Africa, *Atmospheric Chemistry and Physics*,  
18 10, 8783-8801, 10.5194/acp-10-8783-2010, 2010.
- 19 Copeland, R. A., and Crosley, D.: Temperature dependent electronic quenching of OH A<sup>2</sup>Σ,  
20 v'=0 between 230 and 310 K, *Journal of Chemical Physics*, 84, 3099-3105, 1986.
- 21 Creasey, D. J., Halford-Maw, P. A., Heard, D. E., Pilling, M. J., and Whitaker, B. J.:  
22 Implementation and initial deployment of a field instrument for measurement of OH and HO<sub>2</sub>  
23 in the troposphere by laser-induced fluorescence, *J. Chem. Soc.-Faraday Trans.*, 93, 2907-  
24 2913, 1997a.
- 25 Creasey, D. J., Heard, D. E., Pilling, M. J., Whitaker, B. J., Berzins, M., and Fairlie, R.:  
26 Visualisation of a supersonic free-jet expansion using laser-induced fluorescence spectroscopy:  
27 Application to the measurement of rate constants at ultralow temperatures, *Applied Physics B-  
28 Lasers and Optics*, 65, 375-391, 10.1007/s003400050285, 1997b.
- 29 Creasey, D. J., Heard, D. E., and Lee, J. D.: Absorption cross-section measurements of water  
30 vapour and oxygen at 185 nm. Implications for the calibration of field instruments to measure  
31 OH, HO<sub>2</sub> and RO<sub>2</sub> radicals, *Geophysical Research Letters*, 27, 1651-1654,  
32 10.1029/1999gl011014, 2000.
- 33 Edwards, G. D., Cantrell, C., Stephens, S., Hill, B., Goyea, O., Shetter, R., Mauldin, R. L.,  
34 Kosciuch, E., Tanner, D., and Eisele, F.: Chemical Ionization Mass Spectrometer Instrument  
35 for the Measurement of Tropospheric HO<sub>2</sub> and RO<sub>2</sub>, *Analytical Chemistry*, 75, 5317-5327,  
36 2003.
- 37 Faloon, I. C., Tan, D., Leshner, R. L., Hazen, N. L., Frame, C. L., Simpas, J. B., Harder, H.,  
38 Martinez, M., Di Carlo, P., Ren, X. R., and Brune, W. H.: A laser-induced fluorescence  
39 instrument for detecting tropospheric OH and HO<sub>2</sub>: Characteristics and calibration, *J. Atmos.  
40 Chem.*, 47, 139-167, 10.1023/B:JOCH.0000021036.53185.0e, 2004.
- 41 Fittschen, C., Al Ajami, M., Batut, S., Ferracci, V., Archer-Nicholls, S., Archibald, A. T., and  
42 Schoemaeker, C.: ROOOH: a missing piece of the puzzle for OH measurements in low-NO  
43 environments?, *Atmospheric Chemistry and Physics*, 19, 349-362, 10.5194/acp-19-349-2019,  
44 2019.

- 1 Fuchs, H., Bohn, B., Hofzumahaus, A., Holland, F., Lu, K. D., Nehr, S., Rohrer, F., and  
2 Wahner, A.: Detection of HO<sub>2</sub> by laser-induced fluorescence: calibration and interferences  
3 from RO<sub>2</sub> radicals, *Atmospheric Measurement Techniques*, 4, 1209-1225, 10.5194/amt-4-  
4 1209-2011, 2011.
- 5 Fuchs, H., Tan, Z. F., Hofzumahaus, A., Broch, S., Dorn, H. P., Holland, F., Kunstler, C.,  
6 Gomm, S., Rohrer, F., Schrade, S., Tillmann, R., and Wahner, A.: Investigation of potential  
7 interferences in the detection of atmospheric ROx radicals by laser-induced fluorescence under  
8 dark conditions, *Atmospheric Measurement Techniques*, 9, 1431-1447, 10.5194/amt-9-1431-  
9 2016, 2016.
- 10 Gligorovski, S., Strekowski, R., Barbati, S., and Vione, D.: Environmental Implications of  
11 Hydroxyl Radicals (center dot OH), *Chemical Reviews*, 115, 13051-13092,  
12 10.1021/cr500310b, 2015.
- 13 Glowacki, D. R., Goddard, A., Hemavibool, K., Malkin, T. L., Commane, R., Anderson, F.,  
14 Bloss, W. J., Heard, D. E., Ingham, T., Pilling, M. J., and Seakins, P. W.: Design of and initial  
15 results from a Highly Instrumented Reactor for Atmospheric Chemistry (HIRAC),  
16 *Atmospheric Chemistry and Physics*, 7, 5371-5390, 10.5194/acp-7-5371-2007, 2007.
- 17 Hard, T. M., O'Brien, R. J., Chan, C. Y., and Mehrabzadeh, A. A.: Tropospheric free-radical  
18 determination by FAGE, *Environmental Science & Technology*, 18, 768-777,  
19 10.1021/es00128a009, 1984.
- 20 Heard, D. E., and Pilling, M. J.: Measurement of OH and HO<sub>2</sub> in the troposphere, *Chemical*  
21 *Reviews*, 103, 5163-5198, 2003.
- 22 Hofzumahaus, A., Brauers, T., Aschmutat, U., Brandenburger, U., Dorn, H. P., Hausmann, M.,  
23 Hessling, M., Holland, F., PlassDulmer, C., Sedlacek, M., Weber, M., and Ehhalt, D. H.: The  
24 measurement of tropospheric OH radicals by laser-induced fluorescence spectroscopy during  
25 the POPCORN field campaign and Intercomparison of tropospheric OH radical measurements  
26 by multiple folded long-path laser absorption and laser induced fluorescence - Reply,  
27 *Geophysical Research Letters*, 24, 3039-3040, 10.1029/97gl02947, 1997.
- 28 Howard, C. J.: Kinetic measurements using flow tubes, *Journal of Physical Chemistry*, 83, 3-  
29 9, 10.1021/j100464a001, 1979.
- 30 Evaluated Kinetic Data: [www.iupac-kinetic.ch.cam.ac.uk](http://www.iupac-kinetic.ch.cam.ac.uk), 2007.
- 31 Karl, M., Brauers, T., Dorn, H. P., Holland, F., Komenda, M., Poppe, D., Rohrer, F., Rupp, L.,  
32 Schaub, A., and Wahner, A.: Kinetic Study of the OH-isoprene and O<sub>3</sub>-isoprene reaction in the  
33 atmosphere simulation chamber, SAPHIR, *Geophysical Research Letters*, 31,  
34 10.1029/2003gl019189, 2004.
- 35 Malkin, T. L., Goddard, A., Heard, D. E., and Seakins, P. W.: Measurements of OH and HO<sub>2</sub>  
36 yields from the gas phase ozonolysis of isoprene, *Atmospheric Chemistry and Physics*, 10,  
37 1441-1459, 10.5194/acp-10-1441-2010, 2010.
- 38 Mao, J., Ren, X., Zhang, L., Van Duin, D. M., Cohen, R. C., Park, J. H., Goldstein, A. H.,  
39 Paulot, F., Beaver, M. R., Crounse, J. D., Wennberg, P. O., DiGangi, J. P., Henry, S. B.,  
40 Keutsch, F. N., Park, C., Schade, G. W., Wolfe, G. M., Thornton, J. A., and Brune, W. H.:  
41 Insights into hydroxyl measurements and atmospheric oxidation in a California forest,  
42 *Atmospheric Chemistry and Physics*, 12, 8009-8020, 10.5194/acp-12-8009-2012, 2012.
- 43 Marno, D., Ernest, C., Hens, K., Javed, U., Klimach, T., Martinez, M., Rudolf, M., Lelieveld,  
44 J., and Harder, H.: Calibration of an airborne HOx instrument using the All Pressure Altitude-



1 based Calibrator for HO<sub>x</sub> Experimentation (APACHE), *Atmospheric Measurement*  
2 *Techniques*, 13, 2711-2731, 10.5194/amt-13-2711-2020, 2020.

3 Novelli, A., Hens, K., Tatum Ernest, C., Kubistin, D., Regelin, E., Elste, T., Plass-Dülmer, C.,  
4 Martinez, M., Lelieveld, J., and Harder, H.: Characterisation of an inlet pre-injector laser-  
5 induced fluorescence instrument for the measurement of atmospheric hydroxyl radicals,  
6 *Atmos. Meas. Tech.*, 7, 3413-3430, 10.5194/amt-7-3413-2014, 2014.

7 Novelli, A., Hens, K., Tatum Ernest, C., Martinez, M., Nölscher, A. C., Sinha, V., Paasonen,  
8 P., Petäjä, T., Sipilä, M., Elste, T., Plass-Dülmer, C., Phillips, G. J., Kubistin, D., Williams, J.,  
9 Vereecken, L., Lelieveld, J., and Harder, H.: Estimating the atmospheric concentration of  
10 Criegee intermediates and their possible interference in a FAGE-LIF instrument, *Atmos.*  
11 *Chem. Phys.*, 17, 7807-7826, 10.5194/acp-17-7807-2017, 2017.

12 Onel, L., Brennan, A., Gianella, M., Ronnie, G., Aguila, A. L., Hancock, G., Whalley, L.,  
13 Seakins, P. W., Ritchie, G. A. D., and Heard, D. E.: An intercomparison of HO<sub>2</sub> measurements  
14 by fluorescence assay by gas expansion and cavity ring-down spectroscopy within HIRAC  
15 (Highly Instrumented Reactor for Atmospheric Chemistry), *Atmospheric Measurement*  
16 *Techniques*, 10, 4877-4894, 10.5194/amt-10-4877-2017, 2017a.

17 Onel, L., Brennan, A., Seakins, P. W., Whalley, L., and Heard, D. E.: A new method for  
18 atmospheric detection of the CH<sub>3</sub>O<sub>2</sub> radical, *Atmospheric Measurement Techniques*, 10, 3985-  
19 4000, 10.5194/amt-10-3985-2017, 2017b.

20 Onel, L., Brennan, A., Gianella, M., Hooper, J., Ng, N., Hancock, G., Whalley, L., Seakins, P.  
21 W., Ritchie, G. A. D., and Heard, D. E.: An intercomparison of CH<sub>3</sub>O<sub>2</sub> measurements by  
22 fluorescence assay by gas expansion and cavity ring-down spectroscopy within HIRAC  
23 (Highly Instrumented Reactor for Atmospheric Chemistry), *Atmospheric Measurement*  
24 *Techniques*, 13, 2441-2456, 10.5194/amt-13-2441-2020, 2020.

25 Regelin, E., Harder, H., Martinez, M., Kubistin, D., Ernest, C. T., Bozem, H., Klippel, T.,  
26 Hosaynali-Beygi, Z., Fischer, H., Sander, R., Jöckel, P., Königstedt, R., and Lelieveld, J.: HO<sub>x</sub>  
27 measurements in the summertime upper troposphere over Europe: a comparison of  
28 observations to a box model and a 3-D model, *Atmospheric Chemistry and Physics*, 12, 30619-  
29 30660, 2013.

30 Savitzky, A., and Golay, M. J. E.: Smoothing and Differentiation of Data by Simplified Least  
31 Squares Procedures, *Analytical Chemistry*, 36, 1627-1639, 10.1021/ac60214a047, 1964.

32 Schlosser, E., Brauers, T., Dorn, H. P., Fuchs, H., Haeseler, R., Hofzumahaus, A., Holland, F.,  
33 Wahner, A., Kanaya, Y., Kajii, Y., Miyamoto, K., Nishida, S., Watanabe, K., Yoshino, A.,  
34 Kubistin, D., Martinez, M., Rudolf, M., Harder, H., Berresheim, H., Elste, T., Plass-Duelmer,  
35 C., Stange, G., and Schurath, U.: Technical Note: Formal blind intercomparison of OH  
36 measurements: results from the international campaign HO<sub>x</sub>Comp, *Atmospheric Chemistry*  
37 *and Physics*, 9, 7923-7948, 10.5194/acp-9-7923-2009, 2009.

38 Stone, D., Whalley, L. K., and Heard, D. E.: Tropospheric OH and HO<sub>2</sub> radicals: field  
39 measurements and model comparisons, *Chemical Society reviews*, 41, 6348-6404,  
40 10.1039/c2cs35140d, 2012.

41 Wang, G. Y., Iradukunda, Y., Shi, G. F., Sanga, P., Niu, X. L., and Wu, Z. J.: Hydroxyl,  
42 hydroperoxyl free radicals determination methods in atmosphere and troposphere, *J. Environ.*  
43 *Sci.*, 99, 324-335, 10.1016/j.jes.2020.06.038, 2021.

44 Whalley, L. K., Furneaux, K. L., Gravestock, T. J., Atkinson, H. M., Bale, C. S. E., Ingham,  
45 T., Bloss, W. J., and Heard, D. E.: Detection of iodine monoxide radicals in the marine

- 1 boundary layer using laser induced fluorescence spectroscopy, *J. Atmos. Chem.*, 58, 19-39,  
2 2007.
- 3 Whalley, L. K., Blitz, M. A., Desservettaz, M., Seakins, P. W., and Heard, D. E.: Reporting the  
4 sensitivity of Laser Induced Fluorescence instruments used for HO<sub>2</sub> detection to an interference  
5 from RO<sub>2</sub> radicals and introducing a novel approach that enables HO<sub>2</sub> and certain RO<sub>2</sub> types to  
6 be selectively measured, *Atmospheric Measurement Techniques*, 6, 3425-3440,  
7 doi:10.5194/amt-6-3425-2013, 2013.
- 8 Winiberg, F. A. F.: Characterisation of FAGE apparatus for HO<sub>x</sub> detection and application in  
9 an environmental chamber, PhD, School of Chemistry, University of Leeds, Leeds, 2014.
- 10 Winiberg, F. A. F., Smith, S. C., Bejan, I., Brumby, C. A., Ingham, T., Malkin, T. L., Orr, S.  
11 C., Heard, D. E., and Seakins, P. W.: Pressure-dependent calibration of the OH and HO<sub>2</sub>  
12 channels of a FAGE HO<sub>x</sub> instrument using the Highly Instrumented Reactor for Atmospheric  
13 Chemistry (HIRAC), *Atmospheric Measurement Techniques*, 8, 523-540, 10.5194/amt-8-523-  
14 2015, 2015.
- 15 Winiberg, F. A. F., Dillon, T. J., Orr, S. C., Gross, C. B. M., Bejan, I., Brumby, C. A., Evans,  
16 M. J., Smith, S. C., Heard, D. E., and Seakins, P. W.: Direct measurements of OH and other  
17 product yields from the HO<sub>2</sub> + CH<sub>3</sub>C(O)O<sub>2</sub> reaction, *Atmospheric Chemistry and Physics*, 16,  
18 4023-4042, 2016.
- 19 Woodward-Massey, R., Slater, E. J., Alen, J., Ingham, T., Cryer, D. R., Stimpson, L. M., Ye,  
20 C. X., Seakins, P. W., Whalley, L. K., and Heard, D. E.: Implementation of a chemical  
21 background method for atmospheric OH measurements by laser-induced fluorescence:  
22 characterisation and observations from the UK and China, *Atmospheric Measurement*  
23 *Techniques*, 13, 3119-3146, 10.5194/amt-13-3119-2020, 2020.
- 24